Reaction of a Biscationic Distamycin−Ellipticine Hybrid Ligand with DNA. Mode and Sequence Specificity of Binding†

Christian Bailly,*,‡,§ Christine Michaux,|| Pierre Colson,|| Claude Houssier,|| Jian-Sheng Sun,⊥ Thérèse Garestier,⊥ Claude Hélène,⊥ Jean-Pierre Hénichart,# Christian Rivalle,Δ Emile Bisagni,Δ and Michael J. Waring§

Institut de Recherches sur le Cancer, INSERM U124, Place de Verdun, 59045 Lille Cedex, France, Laboratoire de Chimie Macromoléculaire et Chimie Physique, Université de Liège, Liège 4000, Belgium, Laboratoire de Biophysique, Muséum National d'Histoire Naturelle, INSERM U201, CNRS UA481, 43 rue Cuvier, 75005 Paris, France, UCB Pharmaceuticals, Chemin du Foriest, 1420 Braine-l'Alleud, Belgium, Laboratoire de Synthèse Organique, Institut Curie-Biologie, Bât. 110-112, 15 rue G. Clemenceau, 91405 Orsay, France, and Department of Pharmacology, University of Cambridge, Tennis Court Road, Cambridge CB2 1QJ, U.K.

Received June 29, 1994; Revised Manuscript Received September 2, 1994⊗

ABSTRACT: Molecular modeling of complexes between the octanucleotide d(CGATATCG)$_2$ and either a monocationic or biscationic distamycin−ellipticine hybrid molecule predicted that the extra positive charge on the latter conjugate ligand should ensure tight fitting into the minor groove of the duplex without affecting intercalation of the ellipticine chromophore. To test this prediction, we have synthesized a biscationic compound Distel (2+) and investigated its interaction with DNA using various optical and gel electrophoresis techniques. Viscosity, fluorescence lifetime, and circular and linear dichroism measurements bear out the validity of the calculations and show that Distel (2+) does indeed come to lie with its distamycin moiety in the minor groove of DNA and its ellipticine ring intercalated nearby. Linear dichroism experiments with a range of polynucleotides indicate that, unlike its monocationic homologue, the biscationic ligand engages in bidentate binding to AT sequences but not to GC sequences. Footprinting studies employing DNase I and methidiumpropyl-EDTA·Fe^{II} as DNA cleaving agents reveal that the biscationic hybrid is notably selective for AT-rich sequences in DNA. The concentrations required to detect a clear footprint at AT sites with Distel (2+) are 4- to 10-fold lower than those required to produce comparable DNase I footprints with distamycin alone. Also, in accord with the energy-minimized model of the hybrid−oligonucleotide complex, chemical probing experiments using diethyl pyrocarbonate and osmium tetroxide reveal that the hybrid causes significant distortion of the DNA helix, explicable in terms of bending of the duplex toward the minor groove, which greatly enhances the reactivity toward probes in the major groove of the DNA. The experimental results help to identify the determinant factors, predominantly steric and electrostatic interactions, which shape the DNA-binding reaction. Thus, molecular modeling has correctly predicted the DNA-binding properties of a doubly charged ligand and shown that appending an auxiliary basic group onto the distamycin moiety was the right way to proceed in order to convert a nonspecific conjugate into a highly specific DNA reader.

The design of reagents capable of sequence-selective reaction with double-stranded DNA is a critical issue which has long been a topic of interest. Recent exciting discoveries in this field include the development of triple helix-forming oligonucleotides (Thuong & Hélène, 1993), peptide motifs (Churchill & Travers, 1991), and small organic molecules (Dervan, 1986; Nielsen, 1991). Among the four main categories of DNA reactive drugs—intercalating, noncovalent groove binding, cross-linking, and cleaving agents—DNA minor groove binders have been most extensively studied for their capacity to bind to defined sequences in DNA. One of the best known of these agents is the antiviral antibiotic distamycin (Figure 1), which binds selectively to AT-rich sequences in the minor groove of DNA (Zimmer & Wähnert, 1986). The precise structure determination of the distamycin−DNA complex (Kopka et al., 1985; Coll et al., 1987; Pelton & Wemmer, 1990) has provided a sound basis for the development of analogues having the *N*-methylpyrrole rings replaced by different heterocycles containing hydrogen bond acceptor heteroatoms (Lown, 1988). This strategy has been exploited in several attempts to divert the specificity of distamycin from AT to GC sequences and has proved successful in several instances, particularly with the design of imidazole-containing minor groove binders capable of binding to guanine-containing DNA sequences (Lown et al., 1986; Dwyer et al., 1992; Lee et al., 1993). The characterization of the 2:1 distamycin−DNA complex (Pelton & Wemmer, 1989; Fagan & Wemmer, 1992) has provided new opportunities to optimize contacts between the drug and the minor groove of DNA. The affinity of distamycin-like ligands for specific sequences can be enhanced by choosing

† This work was done under the support of research grants (to C.B.) from the INSERM and the ARC; (to C. Houssier) from the FRFC convention 2.4501.91 and the FNRS; (to C. Hélène) from the CNRS and the INSERM; (to E.B.) from the CNRS and the Institut Curie; and (to M.J.W.) from the Wellcome Trust, CRC, and AICR. Support by the "convention INSERM-CFB" is acknowledged.

* Address correspondence to this author.
‡ INSERM U124.
§ University of Cambridge.
|| Université de Liège.
⊥ Muséum National d'Histoire Naturelle.
UCB Pharmaceuticals.
Δ Institut Curie.

⊗ Abstract published in *Advance ACS Abstracts,* November 15, 1994.

0006-2960/94/0433-15348$04.50/0

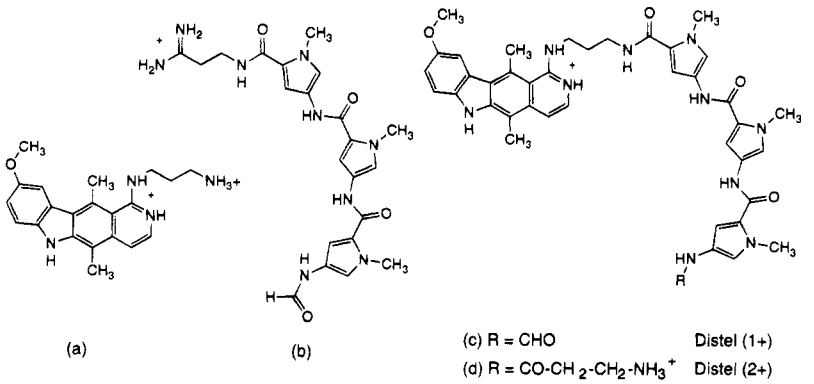

FIGURE 1: Structure of the ellipticine derivative (a), distamycin (b), and the distamycin−ellipticine hybrids, Distel (1+) (c) and Distel (2+) (d). The positive charges on the ligands are indicated.

pairs of ligand molecules with complementary DNA recognition properties (Wade et al., 1993; Geierstanger et al., 1993; Blaskó & Bruice, 1993) and by covalently linking the two DNA-reading elements so as to optimize the geometry of the drug−DNA 2:1 complex (Mrksich & Dervan, 1993; Dwyer et al., 1993).

In parallel, distamycin has been used as a minor groove-targeted carrier for delivering covalently modifying or cleaving reagents to specific sequences in DNA. Over the last few years a growing variety of metal complexes (Schultz et al., 1982; Griffin & Dervan, 1986; Otsuka et al., 1990; Huang et al., 1993), alkylating/cross-linking groups (Krowicki et al., 1988; Church et al., 1990; Broggini et al., 1991; Zhang et al., 1993; He et al., 1993; Tokuda et al., 1993; Xie et al., 1993), and photoactivatable/ionizable functionalities (Matsumoto et al., 1992; Grokhovsky & Zubarev, 1991) have been attached to distamycin-like molecules in order to promote sequence-specific cleavage or bonding to DNA. Another promising prospect for functionalizing minor groove-targeted ligands consists of equipping the DNA-reading element with an intercalating chromophore. This strategy has been mainly exploited in our laboratories with the development of different categories of minor groove binder−intercalator hybrid molecules named combilexins (Bailly & Hénichart, 1991, 1994). Potential advantages of these hybrid molecules are the following: (i) enhancing DNA-binding strength and selectivity, (ii) interfering with topoisomerases, and (iii) facilitating the cellular transport of the drugs, promoting their potential use in cancer chemotherapy.

Recently, we reported the DNA-binding properties of a distamycin−ellipticine hybrid ligand, Distel (1+) shown in Figure 1, which proved to be capable of interacting with DNA via intercalation and minor groove binding but failed to engage in sequence-specific interaction judged by DNase I footprinting experiments (Bailly et al., 1992a). Spectroscopic measurements showed that the binding reaction was largely dominated by the ellipticine chromophore (Bourdouxhe et al., 1992). Molecular modeling studies then suggested that the lack of a positively charged side chain on the distamycin residue appeared to be responsible for the lack of sequence-selective binding. We also deduced that the introduction of a second positive charge on to the distamycin moiety of the molecule would confer much tighter DNA binding (Bourdouxhe et al., 1992).

To verify these theoretical predictions, we have designed and synthesized a biscationic hybrid, Distel (2+) shown in Figure 1, having an aminopropionamido side chain in place of the neutral formamido group of Distel (1+). The extra positive charge on the newly introduced side chain should, at least in theory, provide a tighter anchorage of the drug into the minor groove, providing that the groove binding process does not hinder intercalation of the adjacent ellipticine chromophore. In terms of DNA recognition, the additional positive charge could confer a selectivity for binding to AT-rich DNA sequences by exploiting the higher electronegative potential which exists in the minor groove (Pullman & Pullman, 1981). However, it could also favor nonspecific interactions with the DNA phosphate residues, especially if the molecular shape of the ligand is not well suited for insertion into the narrow minor groove of an AT sequence and/or if the binding of the drug requires extensive distortion of the DNA helix to accommodate such a sterically-demanding composite molecule. It is also worth pointing out that the poor water solubility of the monocationic hybrid prompted us to include a second cationic function so as to improve its solubility and thus the ease of handling of this potential anticancer agent.

The present report is focused on the DNA-binding properties of this distamycin−ellipticine hybrid molecule Distel (2+). We have examined the influence of the second positive charge by addressing the following key questions: does the biscationic hybrid bind to DNA by simultaneous intercalation and minor groove binding, and in contrast to its monocationic homologue, does it selectively recognize defined sequences in DNA? The investigation began with molecular mechanics calculations aimed at discerning the likely molecular basis of the hybrid−DNA interactions and from which the energetic parameters of the Distel (1+)− and Distel (2+)−DNA complexes were obtained. Given these predictive energy-minimized structures, we went on to compare the capacities of the two hybrid molecules to interact with DNA using a range of biochemical and spectroscopic techniques including viscosity, circular dichroism, and fluorescence emission decay measurements. The geometry of the drug−DNA complexes was analyzed by electric linear dichroism using several types of DNA and polynucleotides having varied base composition. The capacity of the biscationic hybrid to recognize specifically certain sequences in DNA was determined using both DNase I and methidiumpropyl-EDTA·Fe^{II} footprinting techniques. In addition, we have used different chemical reagents including diethyl pyrocarbonate and osmium tetroxide to probe at nucleotide resolution the effect of Distel (2+) on the DNA structure. The various experiments reveal unambiguously

that molecular modeling has correctly predicted the behavior of the biscationic hybrid ligand Distel (2+) and that a high degree of sequence-specific recognition has been achieved with this conjugate. Such efficient sequence-specific binding to DNA has never previously been observed with combilexin molecules.

MATERIALS AND METHODS

Drugs. Distamycin A hydrochloride was purchased from Boehringer (Mannheim, Germany); stock solutions were prepared in water. The ellipticine derivative 1-[(3-aminopropyl)amino]-5,11-dimethyl-9-methoxy-6*H*-pyrido[4,3-*b*]carbazole was synthesized as described (Ducrocq et al., 1980). A stock solution (1 mM) of this compound was prepared in methanol. A water-soluble ellipticine derivative containing a diethylamino group in place of the amino group of the ellipticine derivative shown in Figure 1 was used for the viscosity measurements; this ellipticine derivative (BD84) was synthesized as previously described (Larue et al., 1988). The synthesis of the hybrid drug Distel (1+) has been reported (Bailly et al., 1993a). Stock solutions of this compound were prepared in dimethylformamide before subsequent dilutions with water. The synthesis of Distel (2+) will be reported in a chemical communication. The biscationic hybrid is soluble in water and buffers at neutral pH. Methidiumpropyl-EDTA (MPE) was a gift from Professor Peter Dervan (California Institute of Technology, Pasadena, USA). All other chemicals were analytical grade reagents.

Biochemicals. DNA from calf thymus and the double-stranded polymers poly(dA-dT)·poly(dA-dT), poly(dG-dC)·poly(dG-dC), poly(dA)·poly(dT), and poly(dG)·poly(dC) were from Sigma. Their concentrations were determined by applying molar extinction coefficients of 6600, 6600, 8400, 6000, and 7400 M^{-1} cm^{-1}, respectively (Wells et al., 1970). Calf thymus DNA was deproteinized with sodium dodecyl sulfate (protein content <0.2%), and all nucleic acids were dialyzed against 1 mM sodium cacodylate buffer, pH 6.5. The plasmid pUC12 was isolated from *Escherichia coli* by a standard sodium dodecyl sulfate−sodium hydroxide lysis procedure and purified by banding in CsCl−ethidium bromide gradients. The plasmid was cut with *Eco*RI, treated with alkaline phosphatase, and then labeled at the 5′-end using T4 polynucleotide kinase (Pharmacia) and [γ-^{32}P]ATP (6000 Ci/mmol). The linear labeled plasmid was further digested with *Pvu*II to generate the 5′-labeled fragment. For 3′-end labelling, the plasmid was double digested with *Eco*RI plus *Pvu*II for 3 h at 37 °C and then incubated with AMV reverse transcriptase in the presence of [α-^{32}P]dATP (6000 Ci/mmol, New England Nuclear) to label specifically the 3′-end at the *Eco*RI site. The singly end-labeled DNA fragment was then purified by preparative nondenaturing polyacrylamide gel electrophoresis (6.5% acrylamide in TBE buffer: 89 mM Tris base, 89 mM boric acid, and 2.5 mM Na_2 EDTA, pH 8.3). After a rapid autoradiography to locate the DNA, the band was excised from the gel and extracted overnight in 500 mM ammonium acetate and 10 mM magnesium acetate. The purifed 178 base pair *Eco*RI/*Pvu*II restriction fragment was then precipitated twice with 70% ethanol prior to being resuspended in 10 mM Tris and 10 mM NaCl buffer, pH 7.0.

Molecular Modeling. Conformational energy minimization was performed with the JUMNA (Junction Minimization of Nucleic Acids) program package (Lavery, 1988) which uses helicoidal coordinates particularly suitable for nucleic acids. Recent developments of the program package (JUMNA IV) allowed us to include any number of nonbonded ligands in the calculations with the help of the Nchem (Nucleotide Chemistry) program. The ellipticine derivative, distamycin, and Distel conjugate molecules were built using the Insight II graphic program developed commercially by Biosym Inc., and then charged and analyzed by Nchem to prepare a data file containing geometrical parameters, atomic charges, and flexibility information for use in the JUMNA program. Charges of ligands were calculated with a Huckel−Del Re procedure which was parametrized on the basis of quantum mechanical calculations (Lavery et al., 1984). Neither water nor counterions were explicitly included in this calculation. Their effects were simulated by using a sigmoidal distance-dependent dielectric function (Lavery et al., 1986), and by assigning a half charge to the phosphate group.

The first step in the computing procedure required building up the DNA fragment which consisted of eight base pairs in double-helical arrangement [d(GCATATGC)$_2$], positioning the various nucleotides by means of their helicoidal coordinates relative to the global axis system. Helicoidal coordinates were derived from published data obtained by crystallography on the B-DNA double helix (Arnott et al., 1980). In order to create an intercalation site, the rise parameter was increased to 6.8 Å and the twist was subsequently reduced to 16° at the expected site. The interactive docking of the ligand−DNA complex was achieved manually by using Insight II software to avoid steric clashes. In early stages of minimization, the helicoidal variables and/or the sugar−phosphate backbone, as well as ligand variables, could be locked. Minimization was performed by successively decreasing the number of constraints. Finally, all variables were freed to evolve until the energy convergence criterion was reached. The different energy-minimized models were compared to verify that the results were not affected by the order in which the locking variables were released. To ensure that the energy-minimized models were suitable, several starting structures were used: for example, the ellipticine moiety was intercalated at various positions within the double−stranded DNA. The final optimal structure was subsequently subjected to stretching−compression as well as under- and overtwisting deformation by imposing a quadratic constraint on the total rise or twist of the oligomer. This technique ensures the stability of the local minimal energy conformation over an extended range of helicoidal parameters and provides a convenient way to escape the local minimum problem (Poncin et al., 1992a,b). These computations were performed on a Silicon Graphics 4D/420GTXB workstation, and the molecules were visualized with the help of Insight II fully interfaced with JUMNA. The structures obtained after minimization were analyzed by the CURVE program (Lavery & Sklenar, 1989), which determined the helicoidal parameters of all the bases with respect to a global axis derived by the least squares fit.

Viscosity measurements were carried out in a capillary viscometer submerged in a 45 L water bath which was maintained at 25 ±×b10.1 °C. Flow times were measured at least in triplicate to an accuracy of ±0.1 s with a stopwatch, and the average time was calculated. The covalently closed-circular supercoiled pUC12 plasmid DNA was isolated by a sodium dodecyl sulfate−sodium hydroxide

lysis procedure and purified by banding twice in CsCl−ethidium bromide gradients. Aliquots (1−5 μL) of the test drug solution (1−2 mM) were titrated directly into the viscometer containing 2 mL of a solution of the plasmid at various concentrations (125−250 μM). After each addition the solutions were carefully mixed with a small flow of air through the dilution bulb of the viscometer and the flow times measured. Experiments were conducted in buffer containing 10 mM Tris-HCl (pH 7.0) and 10 mM NaCl. Unwinding angles were estimated by reference to an unwinding angle of 26° for ethidium bromide (Wang, 1974) used as a control.

Absorption Spectroscopy. Absorption spectra were recorded on a Perkin-Elmer Lambda 5 spectrophotometer using a 10 mm optical path length. Titrations of the drugs with DNA, covering a large range of drug/DNA phosphate ratios (D/P), were performed by adding aliquots of a concentrated DNA solution to a drug solution at constant ligand concentration (10 μM).

Fluorescence. Static fluorescence measurements were carried out on a Perkin-Elmer LS50 spectrofluorimeter. Fluorescence emission spectra were measured from 330 to 580 nm with an excitation wavelength of 300 nm, and fluorescence excitation spectra were measured from 260 to 440 nm with an emission wavelength of 487 nm. Fluorescence decay measurements were carried out on an Edinburgh Model 199 photon-counting fluorescence instrument. A nitrogen-filled flash lamp was used as light source with emission wavelength set at 450 nm. Appropriate filters were used for both excitation and emission to minimize contributions from light scattering.

Circular dichroism (CD) measurements were recorded on a Jobin-Yvon CD6 dichrograph interfaced to a microcomputer. Solutions of drugs and/or nucleic acids were scanned in 0.5 cm quartz cuvettes. Measurements were made by progressive addition of DNA to a pure ligand solution to obtain the desired drug/DNA ratios. Results are expressed in molar circular dichroism $\Delta\epsilon = \Delta A/lc$, where ΔA is the circular dichroism amplitude, l the cell path length, and c the total ligand concentration.

Electric linear dichroism (ELD) measurements were performed using a computerized optical measurement system (Houssier & O'Konski, 1981). The procedures outlined previously were followed (Houssier, 1981). The optical setup for a high sensitivity T-jump instrument equipped with a Glan polarizer was used under the following conditions: bandwidth 3 nm, sensitivity limit 0.001 in $\Delta A/A$, response time 3 μs. Equations used for the calculation of the different parameters are reported in Houssier (1981) and Bailly et al. (1992b). All experiments were conducted at 20 °C with a 10 mm path length Kerr cell having 1.5 mm electrode separation, in 1 mM sodium cacodylate buffer, pH 6.5. The conductivity of the solutions, measured with a Metrohm conductimeter Model E527, ranged from 0.8 to 1.2 mS. The DNA samples were oriented under a 13 kV/cm electric field, and the drug under test was present at 10 μM together with the DNA or polynucleotide at 100 μM, unless otherwise stated.

To investigate the sequence selectivity by ELD, the reduced dichroism $\Delta A/A$ of a ligand−DNA complex measured in the ligand absorption band must be analyzed with respect to the reduced dichroism measured for the same DNA or polynucleotide at 260 nm in the absence of drug, $(\Delta A/A)^{DNA}$. The dichroism ratio DR is defined as follows: $DR = [(\Delta A/A)^{ligand\text{-}DNA}]/[(\Delta A/A)^{DNA}]$. The numerator refers to the reduced dichroism of the drug−DNA complex measured at the absorption maximum of the ligand bound to DNA. The denominator is always negative under the experimental conditions used. The dichroism ratio is expected to be +1 if the transition moment of the drug chromophore is parallel to the DNA bases, as in the case of complete intercalative binding. For groove binders, the angle between the double-helical axis and the long axis of the chromophore lies below 54°, which gives rise to positive dichroism and thus to a negative DR value. Under these conditions, the reduced dichroism ratios DR for any given drug−DNA and drug−polynucleotide complexes can be mutually compared with good relative accuracy, independent of the polymer size (Bailly et al., 1992b).

DNase I footprinting experiments were performed essentially according to the original protocol of Drew and Travers (1984). Samples (3 μL) of the labeled DNA fragment were incubated with 5 μL of the buffer solution containing the desired drug concentration. After 30−60 min incubation at 37 °C to ensure equilibration, the digestion was initiated by addition of 2 μL of a DNase I solution so as to yield a final enzyme concentration of about 0.01 unit/mL. The extent of digestion was limited to less than 30% of the starting material so as to minimize the incidence of multiple cuts in any strand. After 3 min, the digestion was stopped by addition of 3 μL of an 80% formamide solution containing tracking dyes. Samples were heated at 90 °C for 4 min and chilled in ice for 4 min prior to electrophoresis.

MPE footprinting was carried out according to the procedure initially developed by Van Dyke and Dervan (1983). Briefly, 2 μL of labeled DNA (~500 cps) was mixed with 5 μL of drug at the desired concentration, and the drug−DNA complex was left to equilibrate for at least 30 min at 37 °C. Successively, 1 μL of MPE (100 μM, aliquots stored at −20 °C), 1 μL of a freshly prepared 50 μM solution of $Fe(NH_4)_2(SO_4)_2{\cdot}6H_2O$, and then 1 μL of dithiothreitol (20 mM) were added to initiate the cleavage reaction. After 2 min incubation at room temperature, the reaction was stopped by freeze-drying. Samples were lyophilized and washed at least twice with 50 μL of water. The DNA in each tube was resuspended in 5 μL of formamide−TBE loading buffer, denatured at 90 °C for 4 min, and then chilled in ice for 4 min prior to loading onto the sequencing gel.

Diethyl Pyrocarbonate Reactions. DNA samples were diluted with the drug solution and left to equilibrate for a minimum of 30 min at 37 °C. DPEC (1 μL) was then added, and the mixture was left at room temperature for a further 15 min with frequent mixing (Portugal et al., 1988). The reaction was stopped by adding 200 μL of 0.3 M sodium acetate, and the DNA was precipitated with ethanol and then washed twice with 70% ethanol. The DNA was subsequently cleaved at the modified residues by boiling for 20 min in 1 M piperidine. Samples were lyophilized and resuspended in the gel loading buffer.

Osmium Tetroxide Modification. The reaction was conducted at 0 °C by mixing 35 μL of the preequilibrated drug−DNA solution with 5 μL of a freshly prepared OsO_4/pyridine solution (4/1 v/v) to adjust the final OsO_4 concentration to 2.5 mM. After 15 min at room temperature, the reaction was stopped by extracting the reagent twice with diethyl ether, and the modified DNA was recovered by precipitation with ethanol (McLean & Waring, 1988). After two succes-

Table 1: Conformational Energy Decomposition of the Best Energy-Minimized Drug−d(CGATATCG)$_2$ Complexes

drug−DNA complexes	charges on ligand	ΔE_{DNA}[a]	ΔE_{LIG}[b]	$E_{LIG-DNA}$[c]			E_C[d]
				E_{LJ}	E_{Elec}	E_{tot}	
ellipticine derivative[e]	+2	+34.6	+2.3	−36.0	−53.8	−89.8	−52.9
distamycin	+1	+9.6	+10.8	−59.8	−68.8	−128.6	−108.2
Distel (1+)	+1	+34.2	+11.0	−88.3	−68.4	−156.7	−111.5
Distel (2+)	+2	+34.7	+15.9	−91.3	−96.9	−188.2	−137.6
Distellip[f]	+2	+33.9	+15.7	−93.6	−99.9	−193.5	−143.9

[a] ΔE_{DNA} = deformation energy upon complexation of DNA (kcal/mol). [b] ΔE_{LIG} = deformation energy upon complexation of the ligand. [c] $E_{LIG-DNA}$ = ligand−DNA interaction energy; E_{LJ} = Lennard-Jones component; E_{Elec} = electrostatic component. $E_{tot} = E_{LJ} + E_{Elec}$. [d] $E_C = \Delta E_{DNA} + \Delta E_{LIG} + E_{LIG-DNA}$. [e] The aminopropyl side chain of the ellipticine derivatives is located in the minor groove of the duplex. [f] The computer-designed conjugated called Distellip is made by substituting the *N*-formyl group of Distel (1+) by a guanidinoacetyl group (Bourdouxhe et al., 1992).

sive washes with 70% ethanol and vacuum drying, the DNA samples were treated with piperidine as described above for the DEPC reaction.

Dimethyl sulfate and potassium tetrachloropalladinate reactions were carried out as described (Maxam & Gilbert, 1980; Iverson & Dervan, 1987).

Electrophoresis and Autoradiography. DNA cleavage products were resolved by electrophoresis under denaturing conditions in 8% polyacrylamide gels containing 8 M urea. After 2.5 h electrophoresis at 60 W in TBE buffer, gels were soaked in 10% acetic acid for 15 min, transferred to Whatman 3MM paper, dried under vacuum at 80 °C, and then analyzed on the PhosphorImager. Some of the gels were also subjected to autoradiography at −70 °C with an intensifying screen.

Quantitation by Storage Phosphor Technology Autoradiography. Photostimulable storage phosphor imaging plates (Kodak storage phosphor screens obtained from Molecular Dynamics) were pressed flat against dried sequencing gels and exposed overnight at room temperature. A Molecular Dynamics 425E PhosphorImager was used to collect all data. Base-line-corrected scans were analyzed by integrating all the densities between two selected boundaries using the ImageQuant version 3.3 software.

RESULTS AND DISCUSSION

Computer-Aided Drug Design. Molecular Modeling Analyses of the Distel (1+)− and Distel (2+)−d(CGATATCG)$_2$ Complexes. Previous investigations on Distel (1+) have demonstrated that the two complementary functionalities of this monocationic combilexin permit bidentate binding to DNA, but this is at the expense of DNA sequence selectivity (Bailly et al., 1992a). To help design a novel hybrid of this sort endowed with superior DNA recognition capabilities, we resorted to molecular modeling as a means of determining the geometry and separation of the two linked moieties required to produce optimal DNA sequence recognition. The conformational energy decomposition of the best energy-minimized Distel (1+)−DNA complex led to an understanding of the individual role of each part of the conjugate in the DNA-binding reaction (Table 1). The energy of Distel (1+)−DNA complex formation is only slightly superior to that of the distamycin−DNA complex. The significant increase in the Lennard-Jones component of the ligand−DNA interaction energy as a result of simultaneous intercalation of the ellipticine and minor groove binding of the distamycin part is almost completely lost because of the energy penalty arising from the unstacking of two consecutive base pairs to produce the intercalation site (Bourdouxhe et al., 1992). This study also revealed that the positive charge on the ligand is critical for conferring high affinity for DNA. The replacement of the *N*-formyl group on the distamycin tail of Distel (1+) with a guanidinoacetyl side chain (equivalent to the cationic side chain of netropsin) was predicted to lead to a biscationic hybrid molecule (called Distellip in Table 1) endowed with much higher affinity for DNA.

To verify these predictions, a similar biscationic hybrid, Distel (2+) (Figure 1), bearing a positively charged aminopropionamido side chain in place of the formamido group of Distel (1+), was synthesized. A primary amine was preferred over the guanidinium chain for reasons of chemical synthesis. But prior to synthesis we performed a detailed molecular modeling study in order to evaluate the potentialities of the two attached functional groups. The energy terms for the optimal drug complexes with the octanucleotide d(GCATATGC)$_2$ in the B conformation are summarized in Table 1. In the best energy-minimized drug−DNA complexes, distamycin or the distamycin-like tris-pyrrole moiety of each hybrid resides in the minor groove of the alternating A·T region, and the ellipticine moiety intercalates between the last A·T base pair and the next G·C base pair (i.e., at the 5′-TpG step). The aminopropyl side chain of the ellipticine derivative was previously shown to locate preferentially in the minor groove (Bourdouxhe et al., 1992). The complexation energy E_C for the biscationic ligand Distel (2+) is slightly higher than that calculated for the computer-designed ligand Distellip but remains substantially superior to that calculated for the monocationic ligand Distel (1+). In other words, the amidino side chain of Distellip would provide a better anchorage of the molecule in the minor groove than the amino side chain of Distel (2+), but the latter conjugate is, energetically speaking, preferable over the neutral formamido group of distamycin.

The comparative energy terms in Table 1 merit closer examination. First, the electrostatic component E_{Elec} is significantly higher for Distel (2+) compared to Distel (1+). This is not really surprising, for the minor groove of the central ATAT site must present a deeply negative molecular electrostatic potential which offers an appropriate fit to the bis-charged ligand. Second, the Lennard-Jones energy term is about 3 kcal/mol more negative for Distel (2+) than for Distel (1+). Because of its strong distance dependence, the LJ component is considered as a measure of the quality of steric fit between the ligand and the DNA target. Therefore, the computation suggests that, irrespective of their difference in charge, Distel (2+) is sterically better adapted to fit into the minor groove of the DNA than Distel (1+). As a result, the interaction energy between Distel (2+) and the octanucleotide ($E_{LIG-DNA}$) is 31 kcal/mol lower than that calculated for the Distel (1+)−oligonucleotide complex. This is a considerable improvement, which may find expression in terms of sequence-specific recognition of DNA. Third, it is interesting that the distortion energy of the target DNA sequence, ΔE_{DNA}, is nearly identical for the two hybrid ligands. The deformation energy necessary to change the conformation of the DNA to accommodate both the inter-

calated ellipticine moiety and the appended minor groove-binding moiety is high but less than that expected from a simple additive effect of distamycin plus the ellipticine derivative. The computation suggests that the two drugs affect the DNA structure similarly, which is borne out by the observation (*vide infra*) that the hybrids enhance similarly the reactivity of conformationally-sensitive chemical probes toward DNA. Fourth, the distortion energy of the ligand, ΔE_{LIG}, is significantly higher for Distel (2+) compared to Distel (1+). Thus, the biscationic hybrid becomes more bent or folded in order to match the shape of the DNA receptor site. The introduction of a longer side chain onto the distamycin moiety promotes flexibility which, as a result, may present better hydrogen bonding possibilities. It is significant that the term ΔE_{LIG} for the hybrid Distel (2+) is very close to the sum ΔE_{LIG}(distamycin) + ΔE_{LIG}(ellipticine derivative), as would be expected for an ideal binding of the composite ligand to DNA in which both moieties adapt their respective conformation so as to provide optimum interaction with the receptor site. Of course, both the ligand and DNA undergo significant conformational changes upon interaction, but favorable contributions from both polar interactions (ionic contacts and hydrogen bonds) and hydrophobic effects (van der Waals contacts) greatly exceed the energetic cost of conformational changes. The complexation energy E_C for the Distel (2+)−DNA complex is 26 kcal/mol lower than that calculated for the Distel (1+)−DNA complex. It should be noted that although the calculations permit valid comparison between the energies for the two hybrid ligands, the energetic parameters are not simply related to the free energy of the system and in consequence binding affinities cannot be calculated directly from the energy values tabulated.

The energy-minimized model of the Distel (2+)−d(CGATATCG)$_2$ complex (Figure 2) shows that the recognition of the DNA requires considerable flexibility in the two parts of the hybrid molecule. The ellipticine chromophore is oriented at an angle of about 65° with respect to the long axis of the DNA duplex. It forces the interbase spacing essentially to double, while the distamycin moiety induces slight opening of the minor groove. As usual, the rise was increased to about 7 Å and the twist reduced to about 15° at the intercalation site, (TpG)•(CpA). It can be seen that the double-stranded DNA fragment is bent toward the minor groove upon binding of Distel (2+). A similar trend was observed for Distel (1+) (Bourdouxhe et al., 1992). The variations of the roll angle at each dinucleotide step in the octanucleotide are reported in Figure 3. The roll angle is considered as a prime parameter for describing DNA bending. The drug-free octanucleotide has a rather symmetrical roll pattern, reflecting its 2-fold symmetry. The pronounced positive roll angle at the central T4pA5 step is abolished upon binding of the ligands. With distamycin, two positive roll angles are located near both ends of the DNA fragment. Conversely, the binding of the ellipticine derivative induces a negative roll in the vicinity of its intercalation site and a positive roll at the opposite side of the duplex. The two hybrid ligands exhibit somewhat similar roll patterns. Distel (2+) induces a very negative roll angle at the intercalation site which reflects the bending of the helix toward the minor groove. The positive roll angle found on the distamycin side is indicative of a bending of the helix toward the major groove. The positive and negative roll angles are separated by about half a turn of the double helix, suggesting that the overall bending of the DNA is cooperative upon binding of the conjugate molecules.

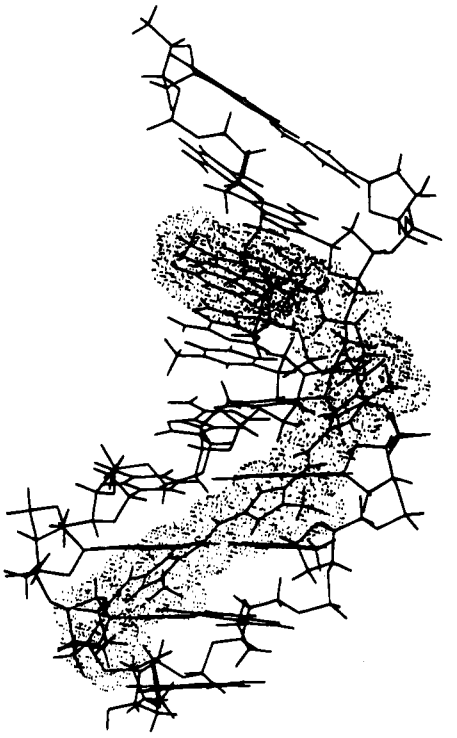

FIGURE 2: View from the minor groove of the best energy-minimized model of the complex between Distel (2+) and d(GCATATGC)$_2$ as calculated by the JUMNA program (Lavery et al., 1984). For clarity, the dot surface representation was used to outline the van der Waals radii of the conjugate molecule. Complex formation induces a pronounced bending toward the minor groove in the vicinity of the ellipticine binding site.

In summary, the computations clearly suggest that the introduction of the new side chain should result in improved DNA binding, mainly due to increased electrostatic attraction between the drug and the DNA at AT-rich sequences with a narrow minor groove. However, an enhancement of the electrostatic component could also favor nonspecific binding of the drug to the negatively charged polymer. There follow a series of complementary biochemical and spectroscopic measurements aimed at determining the mode and sequence selectivity of binding of Distel (2+) to DNA, i.e., at defining the exact influence of the newly introduced cationic side chain on the behavior of the hybrid.

Spectroscopic Changes Observed upon Binding to DNA. The electronic absorption spectrum of Distel (2+) is perturbed on binding to DNA, and metachromatic shifts are observed (Figure 4). Relative to the DNA-free compound, the major UV band centered at 305 nm is red-shifted by about 15 nm and displays considerable hypochromism upon interaction of the drug with DNA. No isosbestic point is observed in the titration of the drug with calf thymus DNA. In these circumstances, attempts to determine a binding constant for the hybrid were unsuccessful; we could not secure any good fit to the data. Equilibrium dialysis experiments also failed because of the strong adsorption of the ligand molecules onto the dialysis membranes. Thus, the interaction of Distel (2+) with calf thymus DNA could not be properly quantitated, but all the indications are that Distel (2+) binds more strongly to DNA than Distel (1+).

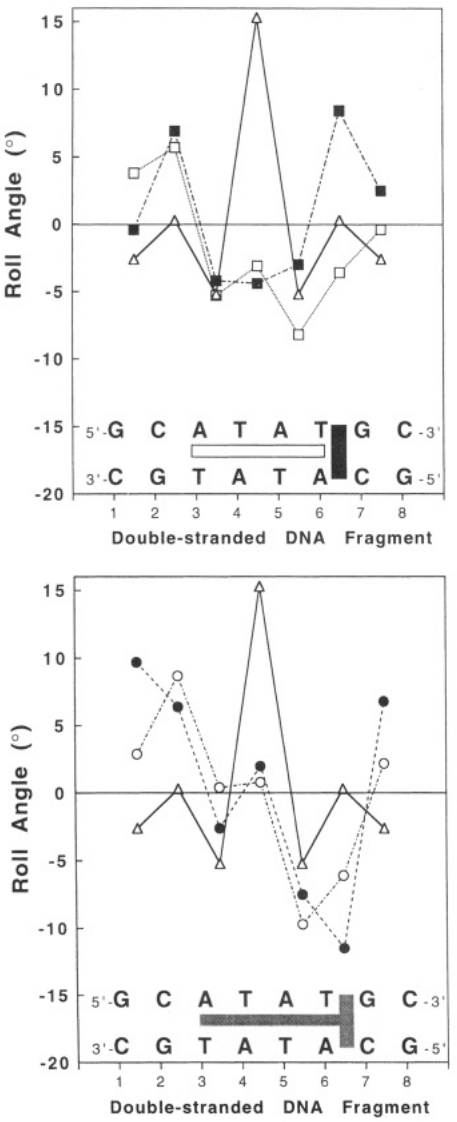

FIGURE 3: Variation of the roll angles along the global helical axis of the double-stranded octanucleotide either uncomplexed (△) or complexed to the ellipticine derivative (□), distamycin (■), Distel (1+) (○) and Distel (2+) (●). The distamycin moiety is located in the minor groove associated with four alternating A·T base pairs, and the ellipticine ring is intercalated between the last A·T base pair and the next C·G base pair (schematized by a horizontal bar and a vertical bar for distamycin and ellipticine moieties, respectively).

Unwinding of Closed Circular Duplex DNA. The ability of a drug to unwind DNA has long been recognized as an important criterion for proving an intercalative mode of binding and has been employed for all classical intercalating drugs (Waring, 1970) including ellipticine (Kohn et al., 1975). Accordingly, to determine whether the chromophore in Distel (2+) unwinds the double helix, we investigated the effects of the biscationic hybrid on the viscosity of supercoiled DNA. The monocationic hybrid could not be tested in this assay because dimethylformamide would be required to prepare the concentrated titrant stock solution of Distel (1+) needed for such experiments, and this organic solvent affects the flow time of the DNA solution in the capillary tube. The assay is possible with the biscationic hybrid because of its superior solubility in purely aqueous buffer. As shown in Figure 5, Distel (2+) removes and reverses the supercoiling of pUC12 DNA. The (water-soluble) ellipticine derivative tested in parallel also causes

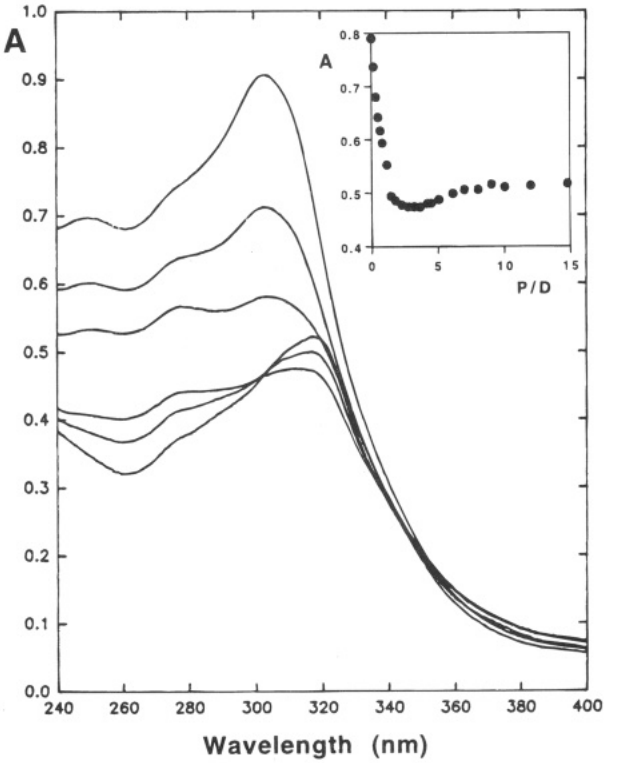

FIGURE 4: Absorption spectra of Distel (2+) in the absence and presence of calf thymus DNA under low ionic strength conditions (1 mM sodium cacodylate buffer, pH 6.5). The figure contains the absorption spectra of the free drug (10 μM), intermediate complexes, and a final complex in which the ligand has been sequestered completely by the DNA. A titration consisted of 15−20 spectral measurements; however, some intermediate spectra have been omitted for clarity. Spectra were referenced against DNA solutions of exactly the same DNA concentration. The DNA phosphateDNA/drug ratio increased as follows (top to bottom curves at 260 nm): 0, 0.5, 1, 3, 6, 15. Inset: Variation of the absorbance at 315 nm with increasing DNA phosphate/drug ratio (P/D).

the decisive removal (increased viscosity) and reversal (decreased viscosity) of supercoiling typical of intercalating agents. The maximum in the plot of flow time as a function of drug concentration occurs when the supercoils are completely removed from the closed circular duplex DNA. The amount of Distel (2+) required to reach this point is 2.3- or 4-fold greater than the amount of ellipticine derivative or ethidium, respectively, required to reach the maximum. This shows that the unwinding of the double helix upon intercalation of a Distel (2+) molecule is less than that of the ellipticine derivative or ethidium by about this factor, given comparably tight binding.

For the ellipticine derivative, the viscometric titration is like that obtained with ethidium bromide as regards the shape of the curve and the flow time corresponding to the fully relaxed circular DNA complex. The equivalence binding ratio, derived from the maxima in the viscosity curves (zero supercoiling), is in the region of 0.08 molecule bound per nucleotide, which leads to an estimated helix-unwinding angle of 19°. A similar unwinding angle was determined in topoisomerase assays for the ellipticine derivative shown in Figure 1 having an (aminopropyl)amino side chain (Bailly et al., 1992a). With the hybrid Distel (2+), we determined the position of the equivalence peak at a range of DNA concentrations in order to estimate the equivalence binding ratio precisely. The plot of Distel (2+) concentration required to relax the supercoiling as a function of DNA

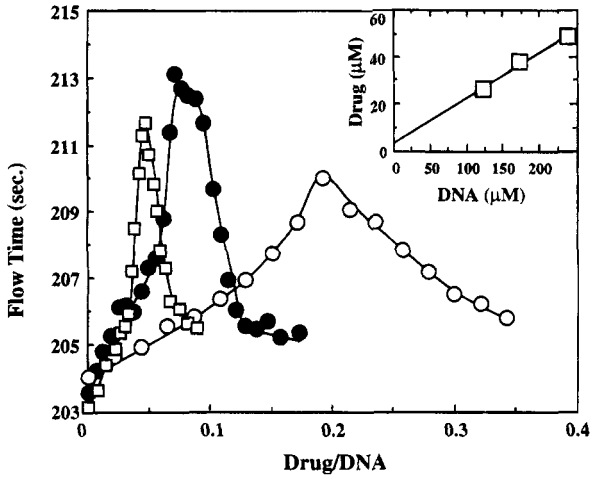

FIGURE 5: Viscometric titrations of pUC12 closed circular duplex DNA with Distel (2+) (○), the ellipticine derivative (●) and ethidium bromide (□). The flow time is plotted as a function of the molar ratio of drug added per DNA nucleotide. Successive aliquots of concentrated drug stock solutions (1 and 2 mM) were added with a calibrated microliter Hamilton syringe into the viscometer containing 2.0 mL of DNA solution (245 μM). The results were corrected for slight changes in DNA concentration during the titration. The inset shows a plot of the concentrations of DNA and Distel (2+) at equivalence (the maxima in the plots of flow time *vs* drug/DNA where supercoiling is removed) from three viscometric titrations starting at different DNA concentrations (Waring & Henley, 1975).

concentration is a straight line (inset in Figure 5). Provided that a simple mass-action interaction is obeyed, the slope of this line is equal to the equivalence binding ratio and the intercept on the ordinate is equal to the free drug concentration in equilibrium with the relaxed circular DNA complex (Révet et al., 1971; Waring & Henley, 1975). Under these conditions, we measured an unwinding angle of 10° for the biscationic hybrid. This angle is well below the value of 26° calculated for ethidium bromide (Wang, 1974) and below the 19° calculated for the ellipticine derivative, but it is close to the value of 11° determined in topoisomerase I assays for the monocationic hybrid (Bailly et al., 1992a). Thus, two independent determinations of helix unwinding by the hybrids give experimentally indistinguishable results: both hybrids are about 50% less effective than the ellipticine derivative in promoting DNA unwinding.

It is worth noting that the plasmid viscosity increase on titration with Distel (2+) is less than that seen with the ellipticine derivative. In addition, we found that in the presence of the hybrid the supercoiling of the DNA does not reverse very efficiently: the viscosity of the positively supercoiled DNA remains higher than that of the negatively supercoiled drug-free DNA sample. These effects could be due to hybrid-induced bending and/or stiffening of the DNA on intercalation of the ellipticine chromophore with its sterically-demanding tris-pyrrole substituent. Changes in the conformation of the DNA appear more evident than with the monocationic hybrid Distel (1+) (Bourdouxhe et al., 1992) and can also be seen in chemical probing experiments (*vide infra*). Drug-induced bending of the helix, as suggested in the molecular modeling described above, has also been postulated with substituted phenanthroline and anthracene derivatives (Gabbay et al., 1973; Wilson et al., 1985a).

The conventional viscometric curve shown in Figure 5 provides *prima facie* evidence for unwinding of the helix induced by the sliding of the ellipticine moiety between adjacent base pairs, but the unwinding angle of both distamycin−ellipticine conjugates is low compared to that of structurally simple intercalating drugs (e.g., ethidium, acridines), although it is comparable to that observed with daunomycin (Waring, 1970). One possible explanation is that two populations of bound ligand molecules coexist: one having the ellipticine moiety intercalated at AT-rich sequences (so as to produce about 19° unwinding) and the other with the ellipticine moiety not intercalated (no unwinding). A low unwinding angle could also be due to extensive buckling of base pairs (Wang, 1993). However, caution must be exercized in interpreting viscometric curves, because other types of interaction with DNA apart from intercalation may cause unwinding (Gale et al., 1981; Hiort et al., 1990). Drug-induced stiffening of DNA will also enhance the viscosity (Strickland et al., 1990). Steroidal diamines, crystal violet, cisplatin, and tris(phenanthroline)ruthenium(II) all unwind DNA but do not intercalate (Waring & Henley, 1975; Wakelin et al., 1981; Blatter et al., 1984; Satyanarayana et al., 1992). Because unwinding of supercoiled DNA does not provide unambiguous proof of intercalation, we performed additional spectroscopic measurements to characterize further the binding of Distel (2+) to DNA. It is always wise to use several complementary techniques to assess an intercalative mode of binding (Gale et al., 1981; Long & Barton, 1990).

Environmental Changes upon Interaction with DNA. The strong fluorescence characteristics of the ellipticine chromophore provide a sensitive spectroscopic handle with which to study its interaction with DNA. The interaction of the hybrid Distel (2+) with calf thymus DNA results in a red shift (about 15 nm) of both the excitation and emission maxima, attributable to the perturbation of the complexed chromophore system on binding to DNA. At the same time, the fluorescence excitation intensity is practically doubled compared to the DNA-free ligand and the emission intensity is increased by 65% (data not shown).

The fluorescence decay profiles of Distel (1+) and Distel (2+), recorded on a time-correlated single photon counting spectrometer, are both bi-exponential in the presence of calf thymus DNA. In fact, deconvolution into two exponential components provides the best fitting of the curves to the experimental data points for both the free and DNA-bound ligand molecules (Figure 6). The extrapolated fluorescence lifetimes of the short- and long-lived components are listed in Table 2 together with their respective intensities. The first thing to notice is the different behavior of unbound Distel (1+) and Distel (2+). The monocationic hybrid exists in solution almost entirely as a single emitting species (the time constant τ_1 accounts for 94% of the amplitude change) whereas the fluorescence decay curves obtained for the biscationic hybrid are true biexponentials, which might suggest the presence of two distinct emitting species. At all events, with both hybrids a substantial lengthening of the fluorescence lifetimes occurs in the presence of DNA. This is consisistent with intercalation of the fluorophore (i.e., the ellipticine ring), as considered in detail elsewhere (Barton et al., 1986; Pyle et al., 1989).

Asymmetry of the Drug Binding Sites. Circular dichroism (CD) measurements of the interaction between Distel (2+) and DNA yielded a set of curves showing two pairs of bands (Figure 7a). The intense negative and positive Cotton effects

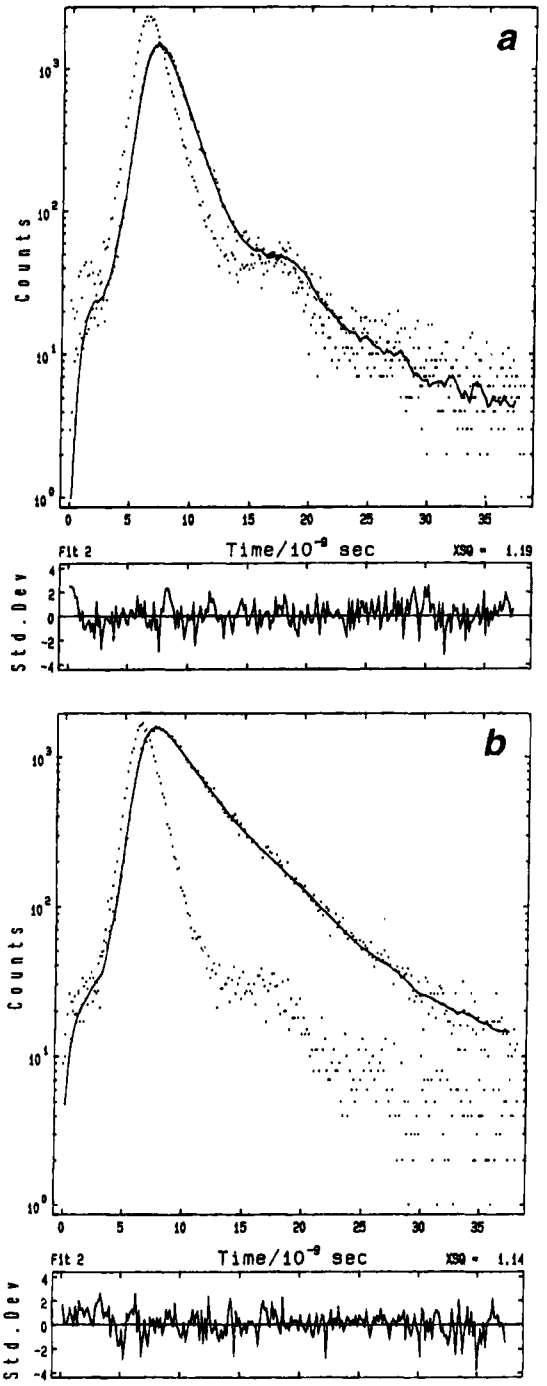

FIGURE 6: Fluorescence decay behavior of the monocationic hybrid Distel (1+) free (a) and bound to calf thymus DNA (b). Dots represent experimental counts, displayed semilogarithmically. The solid curve shows the computer-calculated decay curve obtained from deconvolution of the experimental decay with a double-exponential least-squares fit. Measurements were performed in 1 mM sodium cacodylate, pH 6.5. The relevant parameters are given in Table 2.

observed at 250 and 280 nm, respectively, arise from the DNA molecules (intrinsic CD). This pair of conservative CD bands indicates that the DNA maintains its B conformation upon interaction with the ligand. The weaker negative and positive CD bands centered at 325 and 335 nm, respectively, arise solely from the induction of optical activity in the DNA-bound Distel (2+) molecules (extrinsic CD). The free ligand molecules are optically inactive. The intensity of the second pair of bands increases with the DNA/drug ratio but their amplitude remains about 12-fold weaker than the bands of DNA. Figure 7b shows the variation of the molar dichroism with increasing DNA/drug ratio, for the two hybrids and their parent compounds distamycin and the ellipticine derivative. As reported previously (Bourdouxhe et al., 1992) the CD signals at 320 nm of Distel (1+) and the ellipticine derivative change more or less in parallel. With both ligands the CD first increases until a P/D value of 2.5 is reached and then rapidly decreases to become negligible at P/D > 3. Such evolution of the CD signal may reflect stacking of the drug molecules outside the helix at low P/D ratio followed by intercalation at higher P/D. The CD signals recorded with Distel (2+) are comparable in intensity to those obtained with Distel (1+), but the two hybrids behave differently. Although the signals are relatively weak, the CD evolution with Distel (2+) resembles that observed with distamycin: for both drugs the signal increases as DNA is added to the drug solution up to a roughly constant level. Unfortunately, the drug-induced CD signals are detected in the 300−350 nm region where both the ellipticine moiety and the distamycin moiety absorb light, which tends to complicate the interpretation. However, it is clear that the geometry and asymmetry of the binding sites are different for the two hybrids. The data are consistent with binding models where the interactions of the hybrids Distel (1+) and Distel (2+) with DNA are dominated by the ellipticine and the distamycin moieties, respectively. These observations reinforce the view that the nature of the side chain on the tris-pyrrole residue plays an important role in the DNA-binding reaction and prompted us to perform linear dichroism measurements to gain a more detailed picture of how the hybrid−DNA complex is formed.

Table 2: Fluorescence Emission Lifetimes of the Drugs and Drug−DNA Complexes[a]

	free drug[b]					DNA-bound[c]				
	τ_1[d]	(α_1)[e]	τ_2	(α_2)	$\langle\tau\rangle$[f]	τ_1	(α_1)	τ_2	(α_2)	$\langle\tau\rangle$
Distel (1+)	1.01	(94)	5.77	(6)	1.29	1.05	(20)	4.03	(80)	3.43
Distel (2+)	1.25	(40)	5.45	(60)	3.77	1.82	(38)	8.68	(62)	6.07

[a] Fluorescence decay profiles were fitted satisfactorily ($\chi^2 < 1.2$) by a biexponential model. [b] Drug concentration 10 μM. [c] Calf thymus DNA concentration 100 μM (DNA/drug = 10). [d] τ_1, τ_2 = fluorescence lifetimes in ns. [e] α_1, α_2 = percentage contribution to the fluorescence. [f] $\langle\tau\rangle$ is the average fluorescence lifetime and is given by $\langle\tau\rangle = (\alpha_1\tau_1 + \alpha_2\tau_2)/(\alpha_1 + \alpha_2)$. λ_{em} = 450 nm for the free drugs and 495 nm for the DNA-bound drugs.

Geometry of the Drug−DNA Complexes. Linear dichroism provides a sensitive tool to define the orientation of drugs bound to DNA (Nordén et al., 1992) and has the additional advantage that it senses only the orientation of the polymer-bound ligand: free ligand is isotropic and does not contribute to the signal. We have shown that electric linear dichroism can be particularly useful as a means of analyzing the structure of hybrid molecule−DNA complexes (Bailly et al., 1990, 1992a, 1993a; Flock et al., 1994). Figure 8a shows the ELD spectra of complexes of Distel (1+) and Distel (2+) with poly(dA-dT)·poly(dA-dT). In the 250−290 nm band, which reflects mainly the orientation of the polynucleotide (at P/D = 10), the spectral characteristics of the two hybrid−polynucleotide complexes are identical, suggesting that both drugs exert similar effects on the DNA conformation. The spectra are slightly different in the 300−400 nm region, but in each case the reduced dichroism is negative at 350−400 nm where only the ellipticine moiety absorbs light. The

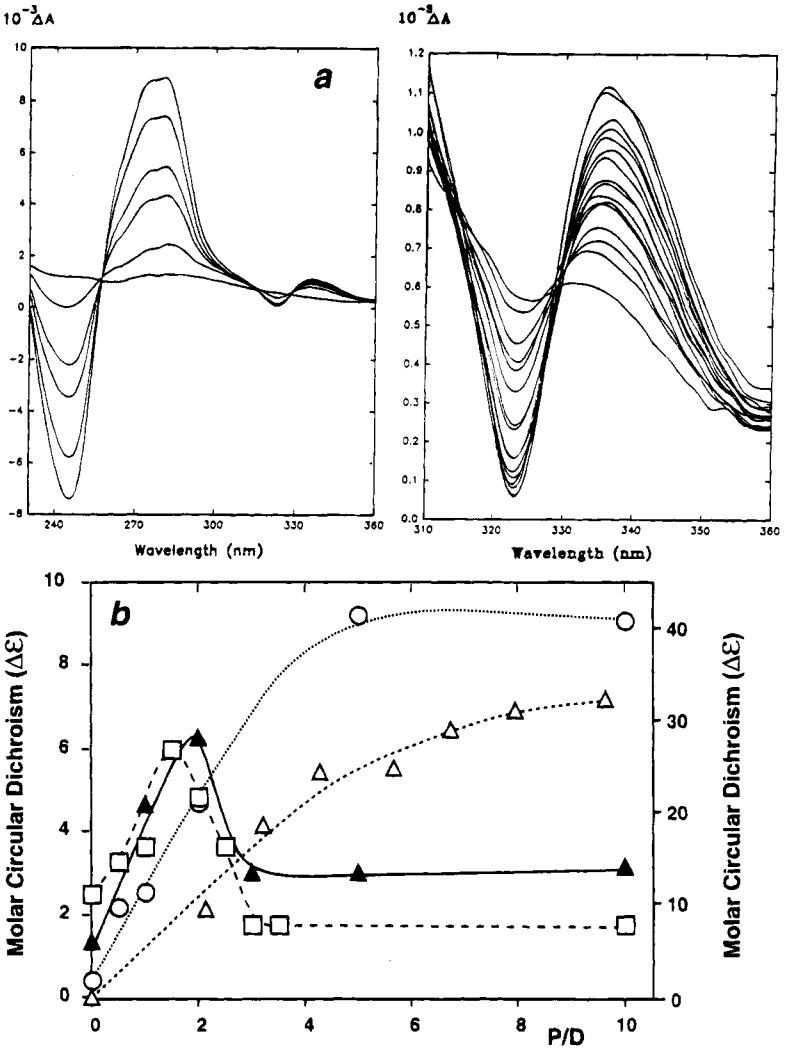

FIGURE 7: Circular dichroism. (a) Titration of Distel (2+) with calf thymus DNA. The DNA phosphate/drug ratio (P/D) varies from 0 to 50 (top to bottom curves at 250 nm). The right panel shows the CD between 310 and 360 nm on an expanded ordinate scale. (b) Variations in molar circular dichroism $\Delta\epsilon$ (ΔA over drug concentration for 1 cm cell path length) with increasing DNA/drug ratio (P/D) for distamycin (○), the ellipticine derivative (□), Distel (1+) (▲) and Distel (2+) (△) bound to calf thymus DNA. λ = 330 nm for distamycin; λ = 320 nm for the ellipticine derivative and the distamycin−ellipticine hybrids. The right scale refers to the curve for distamycin; the left scale refers to the curves for the ellipticine derivative and the two hybrids.

reduced dichroism in the ellipticine band is less negative than that of poly(dA-dT)·poly(dA-dT) alone measured at 260 nm. This indicates that the orientation of the planar chromophore deviates significantly from perpendicularity to the helical axis as expected for a true undisturbed intercalative binding. For Distel (2+), the maximum ELD value in the 360−400 nm band was found to be −0.2, which corresponds to an orientation of the ellipticine chromophore inclined at about 65° to the helix axis. The angle is estimated by comparing the reduced dichroism at a given electric field strength for the DNA bases and for the hybrid in their respective absorption bands, assuming a theoretical angle of 90° for the bases with respect to the orientation axis of the particles (Houssier, 1981). The angle is 62° if an experimental angle of 72° is taken for the bases (Chou & Johnson, 1993). It is remarkable that this angle of 65° coincides exactly with the angle determined from the energy-minimized structure of the Distel (2+)−d(CGATATCG)$_2$ complex (Figure 2), suggesting that the predicted geometry of the hybrid−oligonucleotide complex is correct. The reduced dichroism is positive around 340 nm, clearly indicating that the distamycin moieties of the two conjugates are located in one or another helical groove of the polynucleotide. At 310 nm, the reduced dichroism of the Distel (1+)−poly(dA-dT)·poly(dA-dT) complex is 3-fold more negative than that of the complex with Distel (2+). Although the ellipticine moiety also contributes partially to the absorbance measured at 300−330 nm, in all likelihood this difference is accounted for by a slightly different orientation of the distamycin moiety in each hybrid. As reported previously (Bailly et al., 1992a), the positive ELD value measured at 340 nm with the hybrid-DNA complex corresponds approximately to the sum of the ELD values of the distamycin−DNA and ellipticine−DNA complexes at the same wavelength. So binding of the distamycin part of the hybrid molecule most likely occurs in a similar position to that adopted by the natural unsubstituted antibiotic. Thus the ELD spectrum of the Distel (2+)−polynucleotide complex fully supports the view that the two moieties of the hybrid are engaged in the binding reaction and that the introduction of a positively charged tail onto the distamycin moiety has neither extruded the intercalated ellipticine chromophore from poly(dA-dT)·poly(dA-dT) sequences nor markedly modified the binding geometry or the overall B-DNA conformation.

Recently, we showed that the ELD technique can also be used to gain information about sequence dependence in the

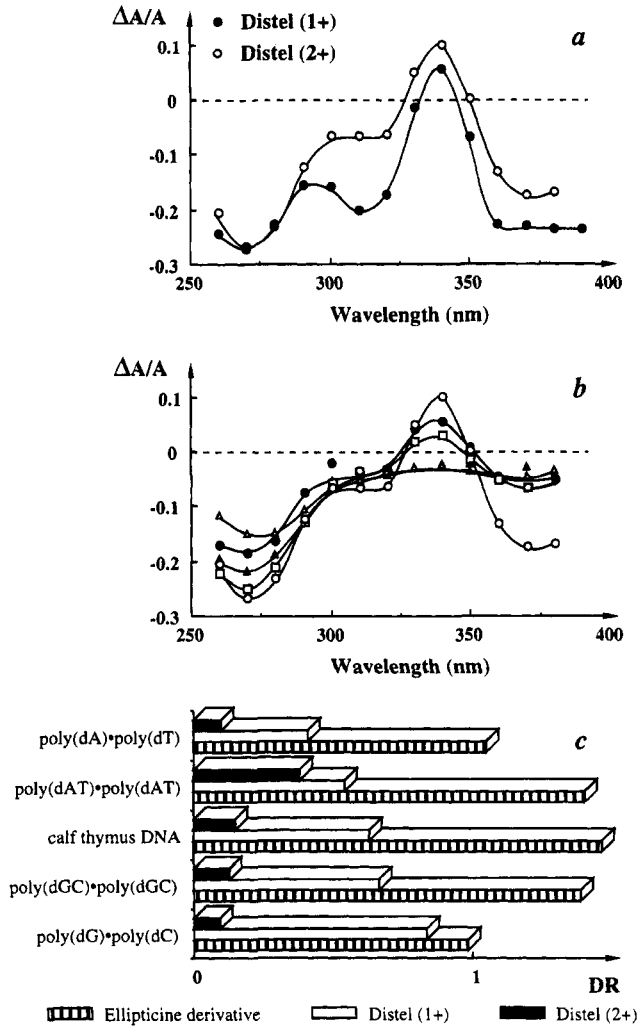

FIGURE 8: Geometry of the drug−DNA complexes inferred from electric linear dichroism. (a) Reduced electric linear dichroism ($\Delta A/A$) spectra of the two distamycin−ellipticine hybrid molecules bound to poly(dA-dT)•poly(dA-dT). (b) Reduced electric linear dichroism ($\Delta A/A$) spectra of the complexes between Distel (2+) and poly(dA-dT)•poly(dA-dT) (○), poly(dA).poly(dT) (●), poly(dG-dC)•poly(dG-dC) (▲), poly(dG)•poly(dC) (△), and calf thymus DNA (□). (c) Variations of the dichroism ratio (DR) of the ellipticine derivative (grey boxes), Distel (1+) (open boxes), and Distel (2+) (black boxes) bound to the polynucleotides of different base composition. DR values were measured at 380 nm for the hybrids and at 310 nm for the ellipticine derivative. ELD data were recorded in the presence of 100 μM polynucleotide and 10 μM drug, in 1 mM sodium cacodylate, pH 6.5, under a field strength of 13 kV/cm.

binding of drugs to DNA (Bailly et al., 1992b). To this end, we examined the binding of the two distamycin−ellipticine hybrids and their parent compounds to calf thymus DNA (which contains 42% G+C residues) and to four polynucleotides with different base composition and/or base pair arrangement. The reduced dichroism spectra of the complexes with Distel (2+) vary considerably according to the GC/AT content of the polymer (Figure 8b). In the presence of poly(dG-dC)•poly(dG-dC) and poly(dG)•poly(dC), the reduced dichroism is very weakly negative and remains constant in the 300−380 nm range, indicating that in this case the ellipticine ring cannot intercalate into the double-helical structure. The weak negative dichroism signals recorded in the presence of these two GC polymers may reflect some nonspecific external attachment of the drug to the DNA helix. The lack of positive reduced dichroism with the two GC polymers indicates that the distamycin moiety of the hybrid ligand is not accommodated within the minor groove of GC sequences, no doubt owing to the constraints produced by the exocyclic 2-amino group of guanine residues projecting into this groove. The 2-amino group of guanine represents a critical recognition element governing the sequence selectivity of many DNA ligands, among which are netropsin and distamycin (Bailly et al., 1993b; Waring & Bailly, 1994).

In the presence of calf thymus DNA and poly(dA)•poly(dT), the ELD spectra exhibit the same positive and negative reduced dichroism signals at 340 and 370 nm seen with poly(dA-dT)•poly(dA-dT), though not so intense, suggesting that in these cases a bimodal binding mechanism involving intercalation and groove binding again takes place. Evidently, alternating $(AT)_n$ sequences provide the best binding sites for the biscationic hybrid ligand.

It is interesting to compare the ELD spectra obtained for Distel (2+) to those previously reported for its monocationic homologue Distel (1+) (Bailly et al., 1993a). This can be seen in Figure 8c where the dichroism ratios DR measured for the complexes of each drug, and of the ellipticine derivative, with five different polynucleotides are presented. DR refers to the reduced dichroism of the drug−DNA complex measured in the absorption band of the test drug (free of contribution from DNA) divided by the dichroism of the DNA measured at 260 nm in the absence of drug (see Materials and Methods). Values of DR for any given drug−DNA and drug−polynucleotide complexes can be mutually compared independently of the polymer size and are representative of the complex geometry (Bailly et al., 1992b). DR values calculated for the ellipticine derivative bound to either poly(dA-dT)•poly(dA-dT), calf thymus DNA, or poly(dG-dC)•poly(dG-dC) are very similar. The same holds true for the monocationic hybrid; the DR values measured in the ellipticine band (at 380 nm) do not vary significantly whether the hybrid is bound to the alternating AT or GC copolymer. Therefore, the binding of these two drugs to AT sites is practically indistinguishable from that to GC sites; their interaction with DNA must be characterized as nonspecific. By contrast, for Distel (2+) the DR ratio corresponding to the poly(dA-dT)•poly(dA-dT) complex is much higher than the DR calculated with the other polynucleotides, suggesting a strong preference for intercalating the ellipticine moiety of Distel (2+) into $(AT)_n$ sequences.

The weak DR values measured for the complexes of Distel (2+) with the homopolymers poly(dA)•poly(dT) and poly(dG)•poly(dC) most probably stem from the unorthodox secondary structure of polypurine−polypyrimidine sequences (Wells et al., 1988). Poly(dG)•poly(dC) adopts a double-helical form which differs from the canonical B-form of DNA (McCall et al., 1985; Heinemann et al., 1992) and appears to be 3 times stiffer than random DNA (Hogan et al., 1983). Poly(dA)•poly(dT) also has unusual properties (Wells et al., 1988). Phased runs of adenine and thymine residues give rise to intrinsically bent DNA (Crothers et al., 1990) and generally are refractory to intercalative binding (Wilson et al., 1985b). Because of their higher rigidity such tracts are unable to accommodate an intercalating chromophore with the same facility as B-form DNA. This seems to be particularly true for Distel (2+), which evidently requires or induces significant distortion of the DNA around the intercalation sites.

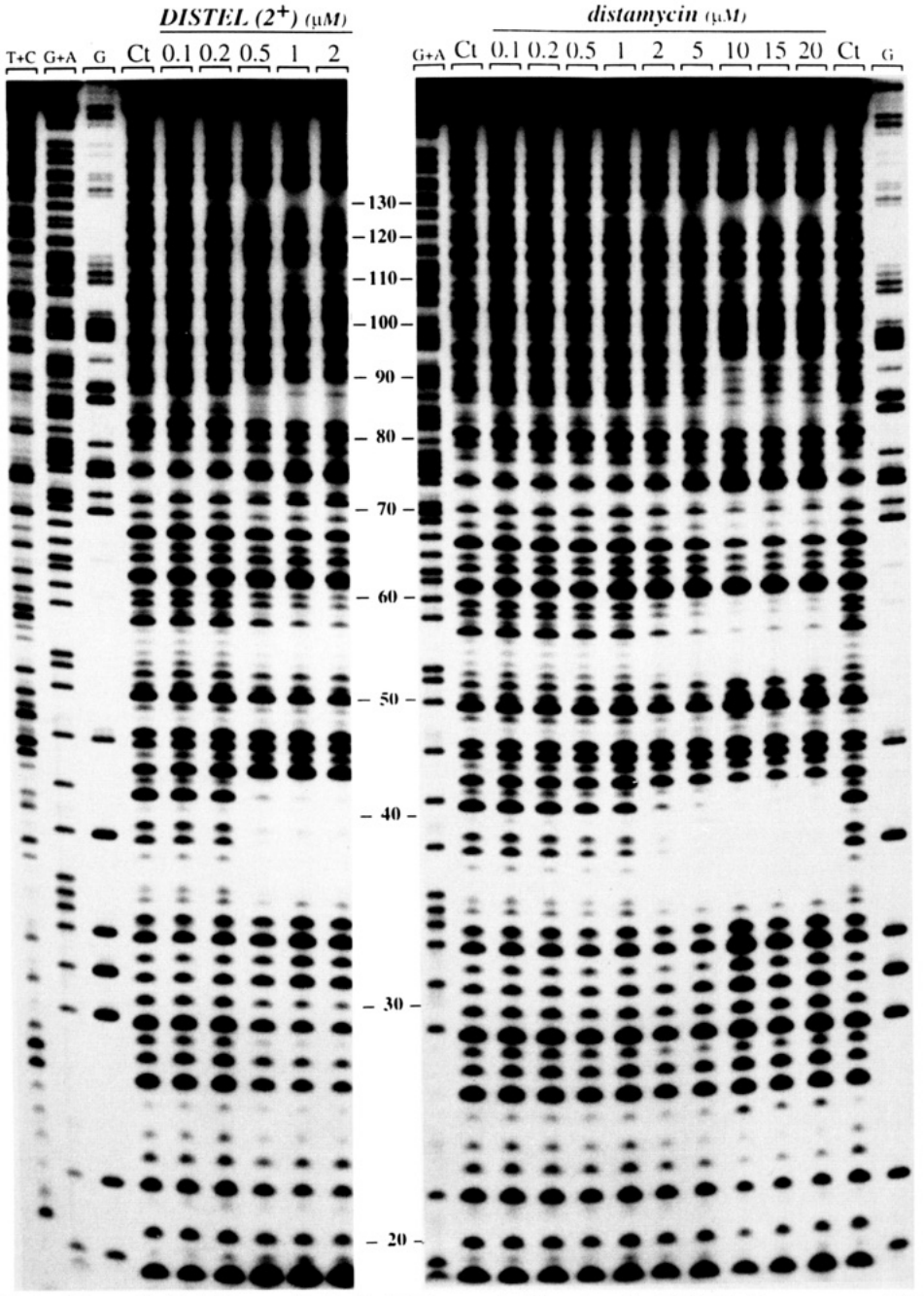

FIGURE 9: DNase I footprinting with the 178-mer *Pvu*II−*Eco*RI fragment of the plasmid pUC12 in the presence of different concentrations of Distel (2+) and distamycin. The DNA was 5′-end labeled at the *Eco*RI site with [γ-^{32}P]ATP in the presence of T4 polynucleotide kinase. The products of DNase I digestion were resolved on an 8% polyacrylamide gel containing 8 M urea. The concentration (μM) of the drug tested is shown at the top of each gel lane. The control tracks labeled "Ct" contained no drug. The tracks labeled "T+C", "G+A", and "G" represent Maxam−Gilbert sequencing markers specific for pyrimidine, purine, and guanine residues respectively. Numbers refer to the sequence shown in the corresponding differential cleavage plot in Figure 10.

To sum up, the ELD data reveal clearly the sequence-dependent nature of Distel (2+)−DNA interactions. GC sequences do not allow the drug to bind in a bidentate fashion. Simultaneous intercalation of the ellipticine ring and groove binding of the distamycin moiety may take place only at AT-containing sequences. This prediction is tested directly in the following footprinting experiments.

Sequence-Selective Binding to DNA. Footprinting was carried out on a 178 base pair restriction fragment obtained by digestion of the plasmid pUC12 with *Eco*RI and *Pvu*II. Two complementary footprinting techniques utilizing deoxyribonuclease I and methidiumpropyl-EDTA·Fe^{II} as DNA-cleaving agents were applied. To illustrate the raw data, an autoradiogram of a DNase I footprinting assay for the binding of distamycin and the hybrid Distel (2+) to the 178-mer restriction fragment is shown in Figure 9. Footprints are very pronounced; it is obvious that the new hybrid binds selectively to certain DNA sequences. There are two essential points to deduce from these experiments. First, in contrast to its predecessor Distel (1+), the biscationic conjugate Distel (2+) recognizes AT-rich sequences in DNA much as distamycin does. Second, the concentration required to produce the footprints is much lower with the hybrid than with distamycin. Depending on the DNA sequence, footprints develop with the hybrid at concentrations 4- to 10-fold lower than those required to elicit a similar extent of footprinting with distamycin. The first point is directly attributable to the presence of a supplementary positive

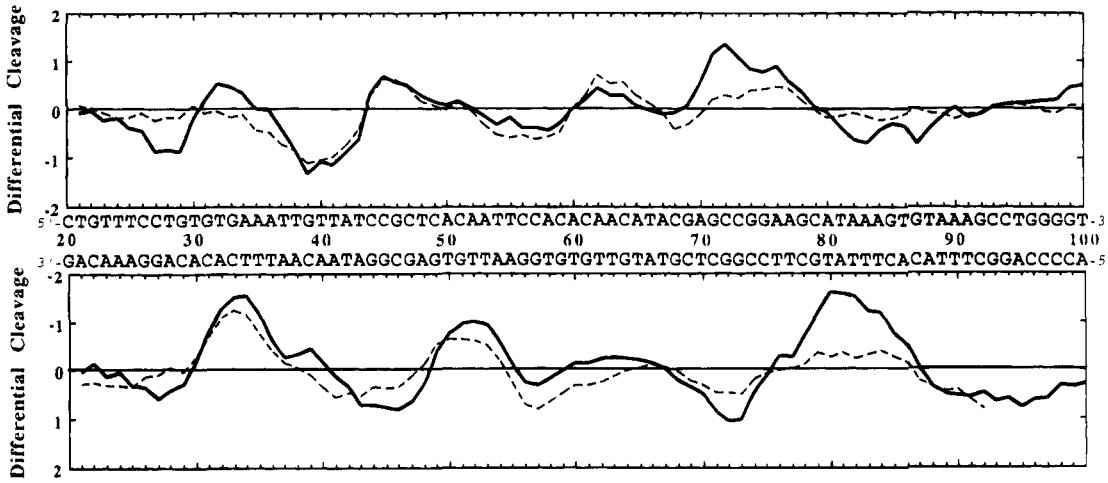

FIGURE 10: Differential cleavage plots showing differences in susceptibility of the 178-mer *Pvu*II-*Eco*RI fragment of the plasmid pUC12 to DNase I cleavage in the presence of 5 μM distamycin (dashed line) and 0.5 μM Distel (2+) (bold line). The upper panel shows differential cleavage of the 5′-labeled strand, the lower panel the complementary 3′-labeled strand. Vertical scales are in units of $\ln(f_a) - \ln(f_c)$, where f_a is the fractional cleavage at any bond in the presence of the drug and f_c is the fractional cleavage of the same bond in the control, given closely similar extents of overall digestion. The ordinate scales for the two strands are inverted, so that the deviation of the points *toward* the lettered sequence (negative values) corresponds to a ligand-protected site and deviation *away* (positive values) represents enhanced cleavage.

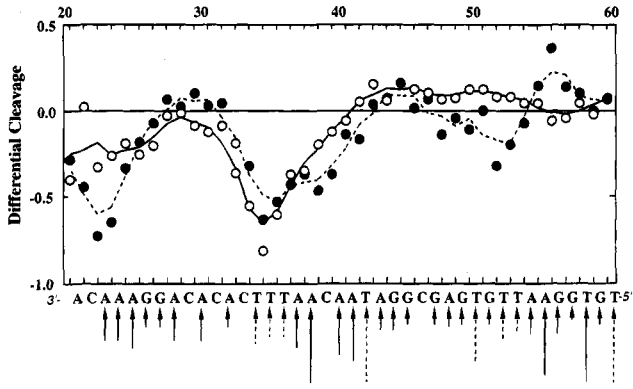

FIGURE 11: Differential cleavage plots showing differences in susceptibility of the 178-mer fragment to MPE·Fe^{II} cleavage in the presence of Distel (2+) at 1 μM (full line) and 10 μM (dashed line). Only the region of the restriction fragment analyzed by densitometry is shown. The arrows below the sequence indicate sites of Distel (2+)-mediated reactivity toward DEPC (full arrows) and OsO_4 (dashed arrows). The lengths of the arrows are proportional to the intensity of cleavage. Other details as for Figure 10.

charge on the molecule: by virtue of its biscationic nature the hybrid binds more strongly to AT-rich sequences. The second point most likely reflects the presence of the ellipticine chromophore, which intercalates in the vicinity of the AT sequence and thus anchors the molecule deeply into the minor groove.

To gain a more quantitative view of the footprints, phosphorimages of the sequencing gels were scanned to derive differential cleavage plots, indicating the relative probabilities of cleavage for each phophodiester bond in the presence of drug. The plots obtained in the presence of 5 μM distamycin and 0.5 μM Distel (2+) superimposed quite well (Figure 10). Both drugs bind selectively to the sequences (all 5′ → 3′) TGAAATTGT (32−40), CAATTC (51−56), and ATAAAGT (80−86), i.e., sequences with at least four consecutive A·T base pairs flanked by a G·C base pair. Complementary analyses using methidiumpropyl-EDTA·Fe^{II} confirmed that the binding sites are generally composed of at least four A·T base pairs (Figure 11). This led to the proposal that the distamycin moiety lies in the minor groove of the $(A{\cdot}T)_n$ stretch with the ellipticine moiety intercalated between the terminal A·T and G·C base pairs, just as depicted in the molecular model shown in Figure 2.

Drug-Induced DNA Conformational Changes. To examine further the consequences of the binding reaction, we carried out a series of chemical probing experiments aimed at detecting drug-induced structural changes in DNA. The reactivity of the 178-mer fragment toward several chemical probes in the presence and absence of Distel (2+) was examined in some detail, the reactivity being detected via the sensitivity of the reacted site to piperidine-catalyzed strand breakage. Neither the standard Maxam−Gilbert reaction of dimethyl sulfate with guanine residues nor the reaction of potassium tetrachloropalladinate with adenine residues was affected by any of the hybrids even at high drug concentrations (not shown). Just as with the large majority of low molecular weight DNA-binding drugs, distamycin and the ellipticine derivative also failed to affect the reaction of either probe within the major groove of DNA. Any alterations in DNA structure induced by the drugs cannot be detected by these two probes. In contrast, the purine-specific alkylator diethyl pyrocarbonate (DEPC) sensitively detects the structural changes in DNA introduced by the binding of the hybrid ligands. Figure 12 shows typical patterns of strand breakage produced by reacting the 178-mer fragment selectively [^{32}P]-labeled on either strand with DEPC in the presence of various concentrations of Distel (2+). It can be seen that the presence of the hybrid provokes strong reaction with the purine residues whereas the drug-free DNA (control lanes) is hardly alkylated, if at all. Reactivity of the N7 position of purines toward DEPC becomes considerably enhanced when DNA adopts an altered conformation, and in particular when the double helix is unwound by drugs (McLean & Waring, 1988; Jeppesen & Nielsen, 1988). The ellipticine derivative and the two hybrid ligands potentiate the reaction of DEPC with the 178-mer DNA fragment to a similar extent. Conversely, distamycin which does not unwind the double helix upon binding has no effect on the reactivity of DNA toward DEPC (Portugal et al., 1988). The drug-induced unwinding of the helix provoked by the intercalation of the ellipticine chromophore

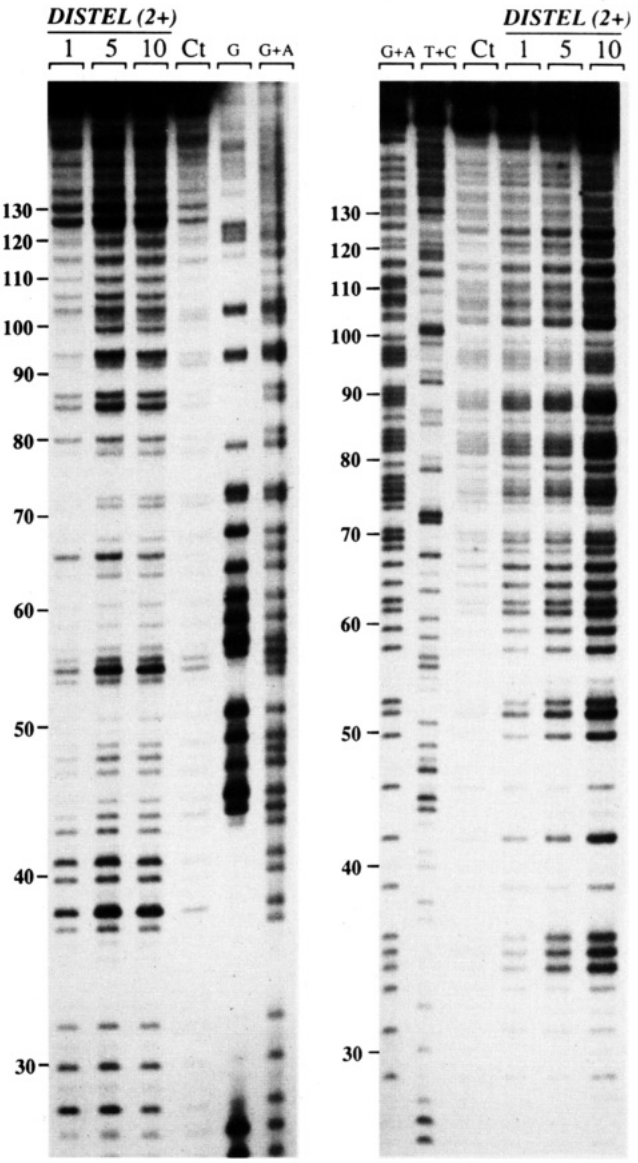

FIGURE 12: Reaction of the 178-mer DNA fragment with diethyl pyrocarbonate in the absence and presence of Distel (2+). Specific strand cleavages occur at DEPC-modified bases in the DNA fragment labeled at its 5′-end (left panel) or 3′-end (right panel). Other details as for Figure 9.

engenders a significant decrease in the base twist angle and consequently an expansion of the major groove of the helix, which should favor the access of DEPC to purine residues in DNA. As surmised for Distel (1+), it is possible that some of the reactivity toward DEPC may also be due to ellipticine-induced DNA bending (Bourdouxhe et al., 1992).

Osmium tetroxide is a useful probe for variations in base stacking induced by the binding of the hybrid drug. Figure 13 shows the reactivity of the 3′-end labeled 178 base pair restriction fragment toward the OsO_4/pyridine complex in the absence and presence of Distel (2+) and the ellipticine derivative. As expected, the probe does not react significantly with native B-DNA in the control lanes whereas its reactivity is markedly enhanced in the presence of either ligand. No such effects occur with distamycin (data not shown), which is known to have no profound effect on DNA structure. The degree of OsO_4 reaction with DNA is dependent on the drug concentration, and Distel (2+) potentiates it much more strongly than the ellipticine derivative, which indicates that the hybrid ligand induces larger distortion of the DNA. This again corroborates the theoretical computations. Osmium tetroxide reacts with DNA via the major groove and oxidizes the 5,6-double bond of thymine residues in a fashion which is particularly sensitive to variation in base stacking. Adduct formation requires out-of-plane attack by the electrophile and is sterically hindered by normal stacking within the double helix (explaining the poor reactivity toward B-DNA). Accordingly, the alteration in reactivity of DNA toward osmium tetroxide could result from base pair destabilization as well as local unwinding of the helix associated with intercalation of the chromophore. However, the ellipticine derivative unwinds the DNA more strongly than Distel (2+) (Figure 5), yet its effect on the reactivity toward osmium tetroxide is weaker than that of the hybrid (Figure 13). This leads us to conclude that it is not the unwinding of the DNA structure induced by intercalation of the ellipticine chromophore which engenders the hypersensitivity toward OsO_4, but rather some perturbation of the stacking interactions between base pairs following the binding of the hybrid. Indeed, the increase in base pair separation, the flattening of the propeller twist, and the change in groove width could all conspire to expose the 5,6-double bond of thymine.

A map of the strand cleavages produced by DEPC and OsO_4 on the 3′-labeled strand of the 178-mer fragment is included in Figure 11 together with the differential cleavage plots determined from MPE•Fe^{II} footprinting experiments. Comparing the sites of reaction of the two chemical probes with the location of the footprints, it appears that DEPC reacts more strongly with adenine residues directly adjacent to binding sites (e.g., A_{38} and A_{55}) than with adenines well outside drug binding sites. By contrast, osmium tetroxide does not react so efficiently with thymine residues within a binding site (e.g., T_{34-36} and T_{52-53}) as with thymines at some distance from binding sites. OsO_4 frequently appears more sensitive to alterations of DNA structure propagated away from drug binding sites (e.g., changes distributed over several nucleotide residues around the intercalation site) than to the disruption of base stacking immediately adjacent to or within the site of intercalation. But it is clear that sites hyperreactive to OsO_4 and DEPC are distributed all along the DNA sequence, indicating that almost the entire secondary structure of the DNA fragment is affected, to varying degrees, by the binding of the conjugate molecule.

CONCLUSION

The present work was focused on three questions: (i) whether intercalation of the charged ellipticine chromophore and minor groove binding of the positively charged tris-pyrrole moiety can take place simultaneously in close proximity; (ii) whether the DNA recognizing element, i.e., the distamycin moiety, retains its specificity for binding to AT-rich sequences when linked to the sterically-demanding intercalating agent; and (iii) whether the intercalating chromophore provides a tight anchorage into DNA without favoring nonspecific binding to DNA. On the basis of the theoretical and experimental data reported here, the answer to all three questions is affirmative.

The results from unwinding of supercoiled DNA (Figure 5), time-resolved fluorescence (Figure 6, Table 2), circular dichroism (Figure 7), and linear dichroism (Figure 8) concur that Distel (2+) is able to bind to AT-rich sequences by

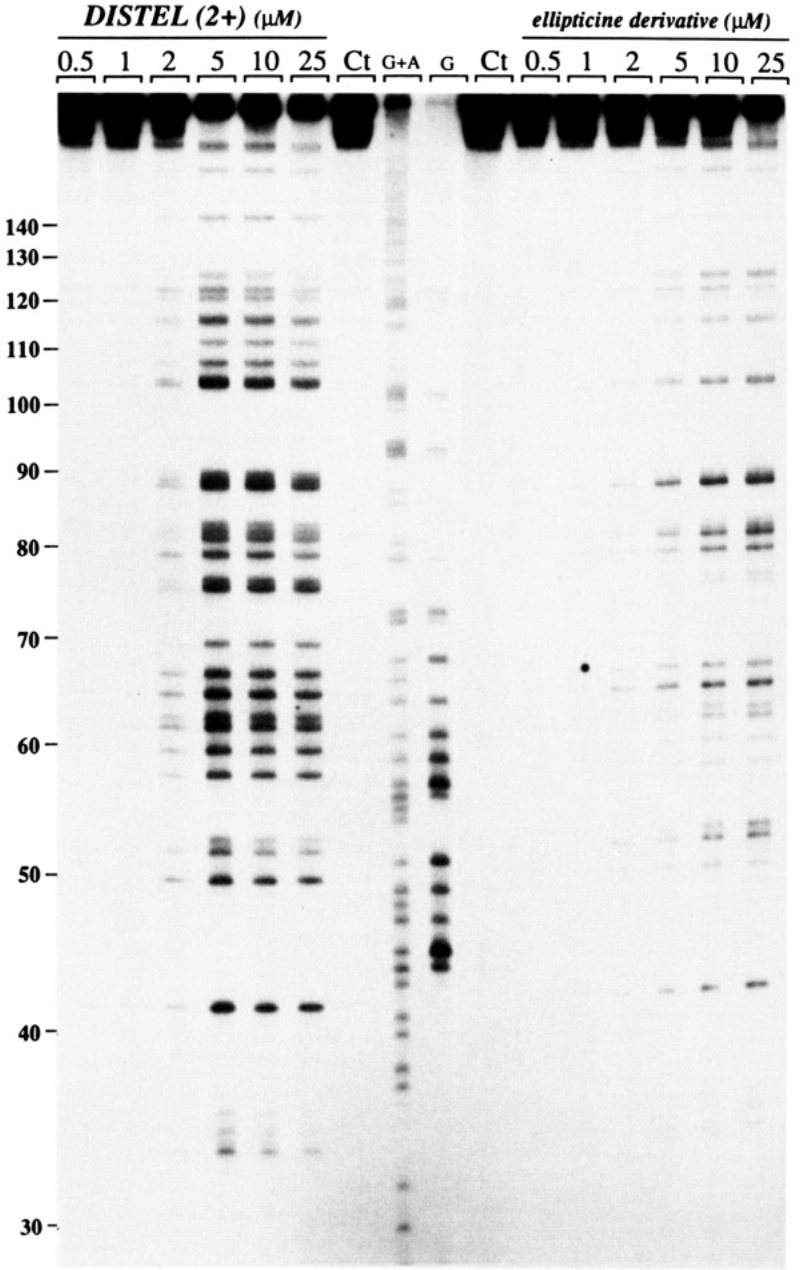

FIGURE 13: Reaction of the 178-mer DNA fragment with the osmium tetroxide/pyridine complex in the presence of Distel (2+) and the ellipticine derivative. Specific strand cleavages are shown at pyridine/OsO_4-modified bases on the 3′-labeled strand of the duplex. Other details as for Figure 9.

intercalation of its ellipticine moiety and minor groove binding of its distamycin moiety. Linear dichroism measurements with different polynucleotides (Figure 8) are consistent with the DNase I (Figure 9) and MPE·Fe^{II} (Figure 11) footprinting data which unambiguously establish that the drug exhibits very pronounced specificity for AT sequences in DNA. As judged from the DNase I footprinting analyses, the AT-specific binding is enhanced by about 1 order of magnitude compared to the parent antibiotic distamycin A (Figure 10). The high affinity of Distel (2+) for AT-rich sequences arises in part from the extra positive charge added to the distamycin tail. However, biscationic analogues of distamycin do not necessarily exhibit a higher affinity for DNA compared to distamycin (Lown et al., 1989). The more significant contribution to the increased strength of interaction comes from the influence of the attached intercalating chromophore which locks the drug into its preferred binding sites. Among the previous hybrid intercalator−minor groove binder ligands we have designed to date (Bailly & Hénichart, 1994), this is the first instance where very high sequence specificity has been achieved [see also the reports of Eliadis et al. (1988) and Subra et al. (1991)].

Our earlier synthesis of the monocationic hybrid Distel (1+) resulted in bidentate binding to DNA, as expected, but without sequence-selective interaction (Bailly et al., 1992a). The introduction of a second positive charge onto the N-terminus of distamycin achieved the desired result by changing the DNA recognition properties of the hybrid without markedly affecting the bimodal binding process. In contrast to Distel (1+) whose ellipticine moiety largely dominates the binding reaction (Bourdouxhe et al., 1992), the interaction of Distel (2+) with DNA seems to be driven as much by the distamycin residue. As a result, although the two ligands have similar hydrogen bonding potentialities, the biscationic hybrid behaves as a sequence-specific ligand while its monocationic analogue is sequence neutral. The

extra positively charged side chain serves to elicit sequence-selective binding, given that the ligand disposes of the adequate structural elements (i.e., hydrogen bond donor and acceptor heteroatoms) required to complement the DNA surface. The results emphasize the contribution of both steric and electrostatic interactions to binding stability and selectivity.

In terms of DNA conformation, the studies reported here agree that double-stranded DNA is highly adaptable and can accommodate a minor groove binding process in close proximity to a more invasive type of binding such as intercalation. The binding of the hybrid to DNA is manifestly sequence-dependent but surely is also structure-dependent. Indeed, the particularly strong binding of Distel (2+) to sequences such as 5′-AAAGT•3′-TTTCA might well be favored by a peculiar local geometry at such sequences. On the one hand, an $(A•T)_n$ tract is believed to present a compression of the minor groove at its 3′-end (Burkhoff & Tullius, 1987), and on the other hand, GT•AC steps present an extremely narrow and deep minor groove (Gochin & James, 1990). Therefore, we are inclined to believe that it may be the local geometry of the site rather than the primary sequence *per se* that is perceived, to a considerable degree, by the drug as an ideal receptor. Other studies have indicated that DNA conformation can be a major factor determining sequence specificity of binding (Laughton et al., 1990), and our recent studies on the kinetics of DNA binding by actinomycin have yielded evidence for a primary structure-dependent recognition of the DNA helix which precedes strict nucleotide sequence recognition (Bailly et al., 1994). Efforts are continuing to discern the best configuration that will permit optimum fitting of Distel (2+) into the minor groove.

REFERENCES

Arnott, S., Chandrasekharan, R., Birsdall, D. L., Leslie, A. G. W., & Ratcliff, R. L. (1980) *Nature 283*, 743−746.

Bailly, C., & Hénichart, J.-P. (1991) *Bioconjugate Chem. 2*, 379−393.

Bailly, C., & Hénichart, J.-P. (1994) *Molecular Aspects of Anticancer Drug−DNA Interactions* Neidle, S., & Waring, M. J., Eds.) Vol. 2, pp 162−196, Macmillan, London.

Bailly, C., Helbecque, N., Hénichart, J.-P., Colson, P., Houssier, C., Rao, K. E., Shea, R. G., & Lown, J. W. (1990) *J. Mol. Recognit. 3*, 26−35.

Bailly, C., OhUigin, C., Houssin, R., Colson, P., Houssier, C., Rivalle, C., Bisagni, E., Hénichart, J.-P., & Waring, M. J. (1992a) *Mol. Pharmacol. 41*, 845−855.

Bailly, C., Hénichart, J.-P., Colson, P., & Houssier, C. (1992b) *J. Mol. Recognit. 5*, 155−171.

Bailly, C., Leclère, V., Pommery, N., Colson, P., Houssier, C., Rivalle, C., Bisagni, E., & Hénichart, J.-P. (1993a) *Anti-Cancer Drug Des. 8*, 145−164.

Bailly, C., Marchand, C. and Waring, M. J. (1993b) *J. Am. Chem. Soc. 115*, 3784−3785.

Bailly, C., Graves, D. E., Ridge, G., & Waring, M. J. (1994) *Biochemistry 33*, 8736−8745.

Barton, J. K., Goldberg, J. M., Kumar, C. V., & Turro, N. J. (1986) *J. Am. Chem. Soc. 108*, 2081−2088.

Blaskó, A., & Bruice, T. C. (1993) *Proc. Natl. Acad. Sci. U.S.A. 90*, 10018−10022.

Blatter, E. E., Vollano, J. F., Krishan, B. S., & Dabrowiak, J. C. (1984) *Biochemistry 23*, 4817−4820.

Bourdouxhe, C., Colson, P., Houssier, C., Sun, J. S., Montenay-Garestier, T., Hélène, C., Rivalle, C., Bisagni, E., Waring, M. J., Hénichart, J.-P., & Bailly, C. (1992) *Biochemistry 31*, 12385−12396.

Broggini, M., Erba, E., Ponti, M., Ballinari, D., Geroni, C., Spreafico, F., & D'Incalci, M. (1991) *Cancer Res. 51*, 199−204.

Burkhoff, A. M., & Tullius, T. D. (1987) *Cell 48*, 935−943.

Chou, P.-J., & Johnson, W. C., Jr (1993) *J. Am. Chem. Soc. 115*, 1205−1214.

Church, K. M., Wurdeman, R. L., Zhang, Y., & Gold, B. (1990) *Biochemistry 29*, 6827−6838.

Churchill, M. E. A., & Travers, A. A. (1991) *Trends Biochem. Sci. 16*, 92−97.

Coll, M., Frederick, C. A., Wang, A. H. J., & Rich, A. (1987) *Proc. Natl. Acad. Sci. U.S.A. 84*, 8385−8389.

Crothers, D. M., Haran, T. E., & Nadeau, J. G. (1990) *J. Biol. Chem. 265*, 7093−7096.

Dervan, P. B. (1986) *Science 232*, 464−471.

Drew, H. R., & Travers, A. A. (1984) *Cell 37*, 491−502.

Ducrocq, C., Wendling, F., Tourbez-Perrin, M., Rivalle, C., Tambourin, P., Pochon, F., & Bisagni, E. (1980) *J. Med. Chem. 23*, 1212−1216.

Dwyer, T. J., Geierstanger, B. H., Bathini, Y., Lown, J. W., & Wemmer, D. E. (1992) *J. Am. Chem. Soc. 114*, 5911−5919.

Dwyer, T. J., Geierstanger, B. H., Mrksich, M., Dervan, P. B., & Wemmer, D. E. (1993) *J. Am. Chem. Soc. 115*, 9900−9906.

Eliadis, A., Phillips, D. R., Reiss, J. A., & Skorobogaty, A. (1988) *J. Chem. Soc., Chem. Commun.*, 1049−1052.

Fagan, P., & Wemmer, D. E. (1992) *J. Am. Chem. Soc. 114*, 1080−1081.

Flock, S., Bailly, F., Bailly, C., Waring, M. J., Hénichart, J.-P., Colson, P., & Houssier, C. (1994) *J. Biomol. Struct. Dyn. 11*, 881−900.

Gabbay, E. J., Scofield, R. E., & Baxter, C. S. (1973) *J. Am. Chem. Soc. 95*, 7850−7857.

Gale, E. F., Cundliffe, E., Reynolds, P. E., Richmond, M. H., & Waring, M. J. (1981) *The Molecular Basis of Antibiotic Action*, John Wiley and Sons Ltd., London.

Geierstanger, B. H., Dwyer, T. J., Bathini, Y., Lown, J. W., & Wemmer, D. E. (1993) *J. Am. Chem. Soc. 115*, 4474−4482.

Gochin, M., & James, T. L. (1990) *Biochemistry 29*, 11172−11180.

Griffin, J. H., & Dervan, P. B. (1986) *J. Am. Chem. Soc. 108*, 5008−5018.

Grokhovsky, S. L., & Zubarev, V. E. (1991) *Nucleic Acids Res. 19*, 257−264.

He, G.-X., Browne, K. A., Groppe, J. C., Blaskò, A., Mei, H.-Y., & Bruice, T. C. (1993) *J. Am. Chem. Soc. 115*, 7061−7071.

Heinemann, U., Alings, C., & Bansal, M. (1992) *EMBO J. 11*, 1931−1939.

Hiort, C., Nordèn, B., & Rodger, A. J. (1990) *J. Am. Chem. Soc. 112*, 1971−1982.

Hogan, M., LeGrange, J., & Austin, B. (1983) *Nature 304*, 752−754.

Houssier, C. (1981) *Molecular Electro-Optics* (Krause, S., Ed.) pp 363−398, Plenum Publishing Corp., New York.

Houssier, C., & O'Konski, C. T. (1981) *Molecular Electro-Optics* (Krause, S., Ed.) pp 309−339, Plenum Publishing Corp., New York.

Huang, L., Morgan, R., & Lown, J. W. (1993) *Bioorg. Med. Chem. Lett. 3*, 1751−1756.

Iverson, B. L., & Dervan, P. B. (1987) *Nucleic Acids Res. 15*, 7823−7830.

Jeppesen, C., & Nielsen, P. E. (1988) *FEBS Lett. 231*, 172−176.

Kohn, K. W., Waring, M. J., Glaubiger, D., & Friedman, C. A. (1975) *Cancer Res. 35*, 71−76.

Kopka, M. L., Yoon, C., Goodsell, D., Pjura, P., & Dickerson, R. E. (1985) *Proc. Natl. Acad. Sci. U.S.A. 82*, 1376−1380.
Krowicki, K., Balzarini, J., De Clercq, E., Newman, R. A., & Lown, J. W. (1988) *J. Med. Chem. 31*, 341−345.
Larue, L., Rivalle, C., Muzard, G., Paoletti, C., Bisagni, E., & Paoletti, J. (1988) *J. Med. Chem. 31*, 1951−1956.
Laughton, C. A., Jenkins, T. C., Fox, K. R., & Neidle, S. (1990) *Nucleic Acids Res. 18*, 4479−4488.
Lavery, R. (1988) *Structure and Expression, Vol. 3, DNA Bending and Curvature* Olson, W. K., Sarma, M. H., Sarma, R. H., Sundaralingam, M., Eds.) pp 191−211, Adenine Press, Guilderland, NY.
Lavery, R., & Sklenar, H. (1989) *J. Biomol. Struct. Dyn. 6*, 655−667.
Lavery, R., Zakrzewska, K., & Pullman, A. (1984) *J. Comput. Chem. 5*, 363−373.
Lavery, R., Sklenar, H., Zakrzewska, K., & Pullman, A. (1986) *J. Biomol. Struct. Dyn. 3*, 989−1014.
Lee, M., Rhodes, A. L., Wyatt, M. D., Forrow, S., & Hartley, J. A. (1993) *Biochemistry 32*, 4237−4245.
Long, E. C., & Barton, J. K. (1990) *Acc. Chem. Res. 23*, 271−273.
Lown, J. W. (1988) *Anti-Cancer Drug Des. 3*, 25−40.
Lown, J. W., Krowicki, K., Bhat, U. G., Skorobogaty, A., Ward, B., & Dabrowiak, J. C. (1986) *Biochemistry 25*, 7408−7416.
Lown, J. W., Krowicki, K., Balzarini, J., Newman, R. A., & De Clercq, E. (1989) *J. Med. Chem. 32*, 2368−2375.
Matsumoto, T., Utsumi, Y., Sakai, Y., Toyooka, K., & Shibuya, M. (1992) *Heterocycles 34*, 1697−1702.
Maxam, A. M., & Gilbert, W. (1980) *Methods Enzymol. 65*, 499−560.
McCall, M., Brown, T., & Kennard, O. (1985) *J. Mol. Biol. 183*, 385−396.
McLean, M. J., & Waring, M. J. (1988) *J. Mol. Recognit. 1*, 138−151.
Mrksich, M., & Dervan, P. B. (1993) *J. Am. Chem. Soc. 115*, 9892−9899.
Nielsen, P. E. (1991) *Bioconjugate Chem. 2*, 1−12.
Nordén, B., Kubista, M., & Kurucsev, T. (1992) *Q. Rev. Biophys. 25*, 51−170.
Otsuka, M., Masuda, T., Haupt, A., Ohno, M., Shiraki, T., Sugiura, Y., & Maeda, K. (1990) *J. Am. Chem. Soc. 112*, 838−845.
Pelton, J. G., & Wemmer, D. E. (1989) *Proc. Natl. Acad. Sci. U.S.A. 86*, 5723−5727.
Pelton, J. G., & Wemmer, D. E. (1990) *J. Am. Chem. Soc. 112*, 1393−1399.
Poncin, M., Hartmann, B., & Lavery, R. (1992a) *J. Mol. Biol. 226*, 775−794.
Poncin, M., Piazzola, D., & Lavery, R. (1992b) *Biopolymers 32*, 1077−1103.
Portugal, J., Fox, K. R., McLean, M. J., Richenberg, J. L., & Waring, M. J. (1988) *Nucleic Acids Res. 16*, 3655−3670.
Pullman, A., & Pullman, B. (1981) *Q. Rev. Biophys. 14*, 289−380.
Pyle, A. M., Rehmann, J. P., Meshoyer, R., Kumar, C. V., Turro, N. J., & Barton, J. K. (1989) *J. Am. Chem. Soc. 111*, 3051−3058.
Révet, B. M., Schmir, M., & Vinograd, J. (1971) *Nature, New Biol. 229*, 10−13.
Satyanarayana, S., Dabrowiak, J. C., & Chaires, J. B. (1992) *Biochemistry 32*, 2573−2584.
Schultz, P. G., Taylor, J. S., & Dervan P. B. (1982) *J. Am. Chem. Soc. 104*, 6861−6863.
Strickland, J. A., Marzilli, L. G., & Wilson, W. D. (1990) *Biopolymers 29*, 1307−1323.
Subra, F., Carteau, S., Pager, J., Paoletti, J., Paoletti, C., Auclair, C., Mrani, D., Gosselin, G., & Imbach, J.-L. (1991) *Biochemistry 30*, 1642−1650.
Thuong, N. T., & Hélène, C. (1993) *Angew. Chem., Int. Ed. Engl. 32*, 666−690.
Tokuda, M., Fujiwara, K., Gomibuchi, T., Hirama, M., Uesugi, M., & Sugiura, Y. (1993) *Tetrahedron Lett. 34*, 669−672.
Van Dyke, M. W., & Dervan, P. B. (1983) *Nucleic Acids Res. 11*, 5555−5567.
Wade, W. S., Mrksich, M., & Dervan, P. B. (1993) *Biochemistry 32*, 11385−11389.
Wakelin, L. P. G., Adams, A., Hunter, C., & Waring, M. J. (1981) *Biochemistry 20*, 5779−5787.
Wang, A. H.-J. (1993) *Molecular Aspects of Anticancer Drug−DNA Interactions* (Neidle, S., & Waring, M. J., Eds.) Vol. 1, pp 32−53, Macmillan, Basingstoke and London.
Wang, J. C. (1974) *J. Mol. Biol. 89*, 783−801.
Waring, M. J. (1970) *J. Mol. Biol. 54*, 247−279.
Waring, M. J., & Henley, S. M. (1975) *Nucleic Acids Res. 2*, 567−586.
Waring, M. J., & Bailly, C. (1994) *Gene* (in press).
Wells, R. D., Larson, J. E., Grant, R. C., Shortle, B. E., & Cantor, C. R. (1970) *J. Mol. Biol. 54*, 465−497.
Wells, R. D., Collier, D. A., Hanvey, J. C., Shimizu, M., & Wohlrab, F. (1988) *FASEB J. 2*, 2939−2949.
Wilson, W. D., Wang, Y.-H., Kusuma, S., Chandrasekaran, S., Yang, N. C., & Boykin, D. W. (1985a) *J. Am. Chem. Soc. 107*, 4989−4995.
Wilson, W. D., Wang, Y.-H., Krishnamoorthy, C. R., & Smith, J. C. (1985b) *Biochemistry 24*, 3991−3999.
Xie, G., Morgan, A. R., & Lown, J. W. (1993) *Bioorg. Med. Chem. Lett. 3*, 1565−1570.
Zhang, Y., Chen, F.-X., Mehta, P., & Gold, B. (1993) *Biochemistry 32*, 7954−7965.
Zimmer, C., & Wähnert, U. (1986) *Prog. Biophys. Mol. Biol. 47*, 31−112.